공학석사 학위논문

# Acoustic wave propagation in Two-dimensional unbounded layered media

## 무한 2층 평면매질 내에서의 음향 파동 전파 이론

**2016년 2 월**

서울대학교 대학원

에너지시스템공학부

김 장 우

# Abstract

Since Pekeris established the theory of wave propagation in acoustic media in 1948, the theory has been crucial in understanding the phenomena of acoustic wave propagation for beginners in geophysics and oceanography. Pekeris theoretically solved the acoustic wave motion problem of unbounded two layers in axially symmetric cylindrical coordinate system. Although his work is mathematically impeccable, his solution is somewhat complicated because it includes a Bessel function, which makes it difficult to calculate numerically. A much simpler solution can be obtained by introducing a two-dimensional plane domain instead of a three-dimensional cylindrical environment. This attempt enables beginners to more intuitively comprehend the characteristics of wave motion in acoustic media and to visualize the wave propagation in acoustic media through modern computer programming. To verify the accuracy of the newly derived two-dimensional solution, the analytical and numerical results are compared, and a regression analysis is performed.

**Keywords : Wave propagation, Unbounded, Acoustic media, Two-dimensional, Contour integration**

**Student Number : 2014-20528**

# Contents

# List of Figures

# List of Tables

# Chapter 1 Introduction

## 1.1 Historical background

The theory of wave propagation in acoustic or elastic media is a foundation for understanding of the behavior of a wave. Even in a complicated seismic section, many seismic events can be interpreted using the concepts of this theory. Thus, beginners in geophysics and oceanography should be familiar with the theory. Pekeris initially established this theory in 1948 by obtaining a normal-mode solution (Pekeris, 1948). He derived a solution in two unbounded media with an explosive point source in an axial symmetrical cylindrical coordinate and compared the findings with experimental results. In 1950, Press and Ewing extended the concepts of this theory to elastic media, and drove a solution in the elastic media and two-layered acoustic-elastic coupled media (Ewing and Press, 1950). Officer treated the acoustic wave propagation theory in his book “Introduction to the Theory of sound transmission with application in the ocean” in 1958, which included a discussion of Pekeris’ work (Officer, 1958). Following Ewing and Officer, Dobrin introduced this theory in his book “Introduction to geophysical prospecting” (Dobrin, 1952), Brekhovskikh and Lurton explained it in their fundamental books for beginners in geophysics (Brekhovskikh, 1991; Lurton, 2002), and Kennett extended the idea to stratified media (Kennett, 1983). Yilmaz mentioned this concept for seismic data analysis (Yilmaz, 2001), and efforts in computational and numerical acoustics with this idea can be found in the books of Jensen and Etter (Jensen, 1997; Etter, 2013). Furthermore, this key theory has been included in many other classic books and papers in geophysics and oceanography as a fundamental concept for wave propagation (DeSanto, 1992; Buckingham, 1992; Katsnelson, 2002; Pujol, 2003; Pilant, 2012).

## 1.2 Purpose

To intuitively comprehend the wave propagation characteristics in acoustic media, visualizing the wave motion of the analytic solution using modern computer programming is particularly useful. Beginners more readily accept these concepts via visualizing the phenomena of wave propagation than by relying solely on mathematical conclusions. The solution obtained from Pekeris' theory is perfect in mathematical terms, but it is complicated and difficult to reproduce the wave motion through numerical calculation. In addition, the two-dimensional approximation solution is utilized for verification of numerical modeling technique because it is difficult to calculate the three-dimensional solution using computer arithmetic. Thus, we focused on the two-dimensional plane domain instead of the three-dimensional solution to simplify the solution and reproduce the wave motion using numerical computations. For the two-dimensional wave equation, a complex Hankel function can be replaced with an exponential function. This substitution makes a seismogram far easier to compute in the time-space domain by taking only two-dimensional Fourier transforms. The solution in frequency-wavenumber is enough to generate the seismogram. Thus, we finished our derivation to obtain the solution in frequency-wavenumber domain.

## 1.3 Application

We also generated the snapshots to easily observe the wave front of each wave event. It is possible to understand of propagation aspects of each wave through the snapshot section. We only deal with the unbounded case in this study, but it can be extended to the problem of bounded case. In bounded problem, there is a normal mode reflection which is reflected to the boundary of the media several times. After deriving the solution of bounded problem, it is possible to simulate the seismic signals under the shallow marine environment. However, the simplicity of the solution makes it difficult to reflect a complex actual physical environment. Above this, this study can be a foundation to the theory of acoustic-elastic coupled and elastic media. Acoustic media is considered for the simplicity of discussion. But there exist elastic effects of ocean bottom layer. Therefore, acoustic-elastic solution can give a much exact model for the ocean system.

In this paper, we used the identical procedures as Pekeris and focused on visualizing the phenomena of wave propagation using computer arithmetic by confining the domain to a two-dimensional plane instead of a three-dimensional cube. To verify the new solution, we compare the results to those of a numerical finite element modeling technique using a least square fitting.

# Chapter 2 Theory

## 2.1 Fundamental solution for the wave equation in the two-dimensional plane domain

The wave equation in a two-dimensional plane domain (x-z) is

$$\nabla^2 u = \frac{\partial^2 u}{\partial x^2} + \frac{\partial^2 u}{\partial z^2} = \frac{1}{c^2}\frac{\partial^2 u}{\partial t^2} \tag{1}$$

where $u$ is the velocity potential. To solve a given problem, we can take a product solution of the equation,

$$u = e^{i\omega t} F(x) G(z) \tag{2}$$

We will consider a simple harmonic point source with a single frequency $\omega$.

Substituting a product solution into equation (1) yields

$$\nabla^2 u = e^{i\omega t}\frac{d^2 F(x)}{dx^2} G(\mathrm{z}) + e^{i\omega t} F(x)\frac{d^2 G(z)}{dz^2} = -\frac{\omega^2}{c^2} e^{i\omega t} F(x) G(z) \tag{3}$$

After a simple reduction, we obtain

$$\frac{d^2 F(x)}{dx^2}\frac{1}{F(x)} = -\frac{d^2 \mathrm{G(z)}}{dz^2}\frac{1}{\mathrm{G(z)}} - \frac{\omega^2}{c^2} \tag{4}$$

The left side of equation (4) is independent of $z$, and the right side of equation (4) is independent of $x$. To satisfy the equality of each side for any value of $x$ and $z$, equation (4) on each side must be equal to a constant $-k^2$. Thus, we have

$$\frac{d^2F(x)}{dx^2} + k^2F(x) = 0$$
$$\frac{d^2G(z)}{dz^2} + \left(\frac{\omega^2}{c^2} - k^2\right)G(z) = 0 \tag{5}$$

The fundamental solution of $F(x)$ and $G(z)$ can be represented as

$$F(x) = e^{\pm ikx}$$
$$G(z) = e^{\pm i\beta z} \quad \text{where} \quad \beta = \left(\frac{\omega^2}{c^2} - k^2\right)^{1/2} \tag{6}$$

Finally, the velocity potential $u$ can be expressed as

$$u = F(x)G(z)e^{i\omega t} = e^{\pm ikx}e^{\pm i\beta z}e^{i\omega t} \tag{7}$$

## 2.2 Physical solution for the wave equation in the two-dimensional plane domain

Now, let us consider the following physical domain. The physical properties of the acoustic media for the wave propagation problem to be solved are shown in Figure 1 (Pekeris, 1948).

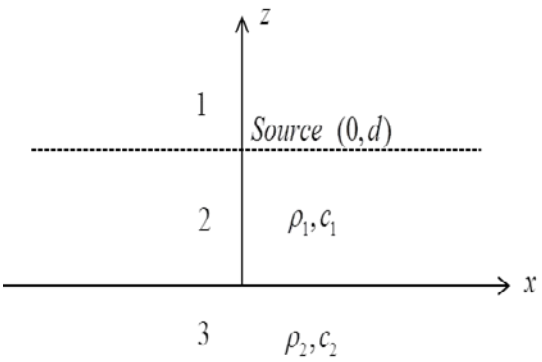


Figure 1. This is the physical properties of the acoustic media for the wave propagation problem to be solved are shown in Figure 1 (Pekeris, 1948).

A point source exists at $x = 0, z = d$. There is a plane boundary at $z = 0$ between two media of velocities $c_1$ and $c_2$ and densities $\rho_1$ and $\rho_2$, respectively. The fundamental solution of the wave equation in the two-dimensional domain is

$$u = F(x)G(z)e^{i\omega t} = G(z)e^{\pm ikx}e^{i\omega t} \tag{8}$$

The form of $G(z)$ for each area of Figure 1 is

$$
\begin{aligned}
G_1 &= Ae^{-i\beta_1 z} + Ee^{i\beta_1 z} \qquad z > d \\
G_2 &= Be^{-i\beta_1 z} + Ce^{i\beta_1 z} \qquad 0 \le z \le d \\
G_3 &= De^{i\beta_2 z} + Fe^{-i\beta_2 z} \qquad z < 0
\end{aligned} \tag{9}
$$

where $\beta_1 = \sqrt{\frac{\omega^2}{c_1^2} - k^2} = \sqrt{k_1^2 - k^2}$, $\beta_2 = \sqrt{\frac{\omega^2}{c_2^2} - k^2} = \sqrt{k_2^2 - k^2}$.

where the subscript number of $G(z)$ indicates each area in Figure 1.

Constant $E$ should be zero to avoid the unreasonable physical condition of an exponential increase of $G_1$ with positive $z$. With an identical approach, $F$ should be zero to avoid blowing up of $G_3$ with negative $z$.

To ensure that there are outgoing waves from the point source and satisfy the boundary condition between two media, the value of $\beta(\beta_1, \beta_2)$ should be determined to be either positive real or negative imaginary, depending on the value of $k$.

Our solution must comply with boundary condition at the interface between two media and near the source. The continuity of pressure and vertical particle velocity should be satisfied at the interface $z = 0$.

$$
\begin{cases}
\rho_1 G_2 = \rho_2 G_3 \\
dG_2 / dz = dG_3 / dz
\end{cases} \quad at\ z = 0 \tag{10}
$$

In addition, we impose the continuity of pressure and discontinuity of vertical particle velocity on the plane $z = d$ at the depth of the source.

$$
\begin{cases}
G_1 = G_2 \\
\dfrac{dG_2}{dz} - \dfrac{dG_1}{dz} = 2
\end{cases} \quad at\ z = d \tag{11}
$$

The particle velocity of the point source is assumed to be 2 instead of 1 to simplify the calculation.

These conditions can be represented in a matrix form, and we obtain

$$\begin{pmatrix} 0 & \rho_1 & \rho_1 & -\rho_2 \\ 0 & -\beta_1 & \beta_1 & -\beta_2 \\ e^{-i\beta_1 d} & -e^{-i\beta_1 d} & -e^{i\beta_1 d} & 0 \\ e^{-i\beta_1 d} & -e^{-i\beta_1 d} & e^{i\beta_1 d} & 0 \end{pmatrix} \begin{pmatrix} A \\ B \\ C \\ D \end{pmatrix} = \begin{pmatrix} 0 \\ 0 \\ 0 \\ 2/i\beta_1 \end{pmatrix} \tag{12}$$

Each coefficient is determined by solving the matrix. Using Cramer's rule, we obtain

$$\begin{aligned} A &= \frac{1}{i\beta_1}\left( e^{i\beta_1 d} + \left( \frac{\beta_1 - b\beta_2}{\beta_1 + b\beta_2} \right) e^{-i\beta_1 d} \right) \\ B &= \frac{1}{i\beta_1}\left( \frac{\beta_1 - b\beta_2}{\beta_1 + b\beta_2} \right) e^{-i\beta_1 d} \\ C &= \frac{1}{i\beta_1} e^{-i\beta_1 d} \\ D &= \frac{1}{i\beta_1}\left( \frac{2b\beta_1}{\beta_1 + b\beta_2} \right) e^{-i\beta_1 d} \end{aligned} \tag{13}$$

where $b = \rho_1 / \rho_2$ , density ratio.

With each coefficient, $G(z)$ can be determined as

$$\begin{aligned} G_1(z) &= \frac{1}{i\beta_1}\left( e^{i\beta_1 d} + \left( \frac{\beta_1 - b\beta_2}{\beta_1 + b\beta_2} \right) e^{-i\beta_1 d} \right) e^{-i\beta_1 z} \\ G_2(z) &= \frac{1}{i\beta_1}\left( \frac{\beta_1 - b\beta_2}{\beta_1 + b\beta_2} \right) e^{-i\beta_1 d} e^{-i\beta_1 z} + \frac{1}{i\beta_1} e^{-i\beta_1 d} e^{i\beta_1 z} \\ G_3(z) &= \frac{1}{i\beta_1}\left( \frac{2b\beta_1}{\beta_1 + b\beta_2} \right) e^{-i\beta_1 d} e^{i\beta_2 z} \end{aligned} \tag{14}$$

Consequently, substituting equation (14) into equation (8) and integrating from $-\infty$ to $\infty$ with respect to $k$, we obtain the velocity potential in each region.

$$
\begin{aligned}
u_1 = e^{i\omega t}\phi_1(x,z,\omega) &= e^{i\omega t}\int_{-\infty}^{\infty}\frac{1}{i\beta_1}e^{\pm ikx}e^{-i\beta_1(z-d)}dk \\
&\quad + e^{i\omega t}\int_{-\infty}^{\infty}\frac{1}{i\beta_1}\left(\frac{\beta_1-b\beta_2}{\beta_1+b\beta_2}\right)e^{\pm ikx}e^{-i\beta_1(z+d)}dk \\
u_2 = e^{i\omega t}\phi_2(x,z,\omega) &= e^{i\omega t}\int_{-\infty}^{\infty}\frac{1}{i\beta_1}e^{\pm ikx}e^{-i\beta_1(d-z)}dk \\
&\quad + e^{i\omega t}\int_{-\infty}^{\infty}\frac{1}{i\beta_1}\left(\frac{\beta_1-b\beta_2}{\beta_1+b\beta_2}\right)e^{\pm ikx}e^{-i\beta_1(d+z)}dk \\
u_3 = e^{i\omega t}\phi_3(x,z,\omega) &= e^{i\omega t}\int_{-\infty}^{\infty}\frac{1}{i\beta_1}\left(\frac{2b\beta_1}{\beta_1+b\beta_2}\right)e^{\pm ikx}e^{-i(\beta_1 d-\beta_2 z)}dk
\end{aligned}
\tag{15}
$$

The first integral of $u_1$ and $u_2$ implies a direct wave from the source to the receiver, and the second denotes the refraction and reflection wave events. The integral of $u_3$ involves a wave traveling across the interface between two media. The second integral of $u_1$ and $u_2$ are identical, but the first integrals of $u_1$ and $u_2$ are different in terms of the signs of $z$ and $d$, depending on the position of the source and the receiver. The quantity in parentheses of $u_1$ and $u_2$ is the Rayleigh reflection coefficient, which indicates the energy ratio rebounded from the boundary to the lower medium. The quantity in parentheses of $u_3$ is the Rayleigh refraction coefficient, which indicates the energy ratio transmitted to the upper medium. In this paper, we only consider the case involving a refraction wave (head wave).

To visualize the wave motion, we generated the seismogram for the velocity potential $u_2$ using computer arithmetic. Because $u_2$ is given in the frequency-wavenumber domain, we obtained a solution in time-space by taking two-dimensional inverse Fourier transforms in terms of $k$ and $\omega$. The Figure 2 shows a seismogram on the two-dimensional plane.

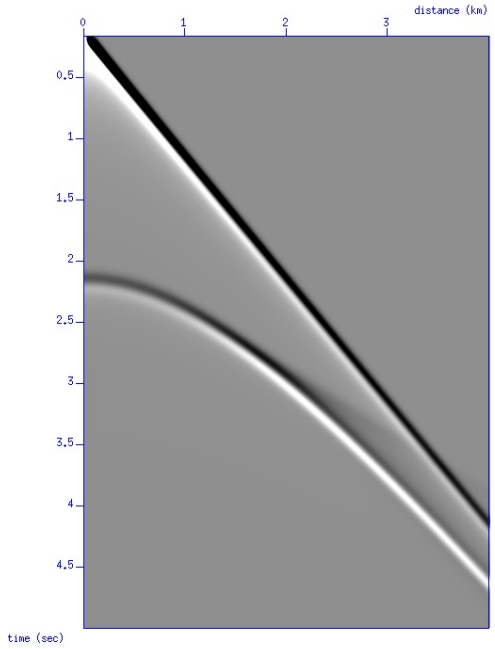


Figure 2. A seismogram of $u_2$. Using the algorithm of inverse Fourier transforms, the solution in the time-space domain can be obtained.

The depth of the source and array of receivers is 1 km from the interface, and the offset varies from 0 km to 4 km along the x-axis. The first derivative of the Gaussian function was applied as a source wavelet. The velocities of the top and bottom layers are 2 and 1 km/s, respectively. We clearly observe a direct wave, a reflection wave, and a refraction wave (head wave).

The Figure 3 shows the snapshots on the two-dimensional plane.

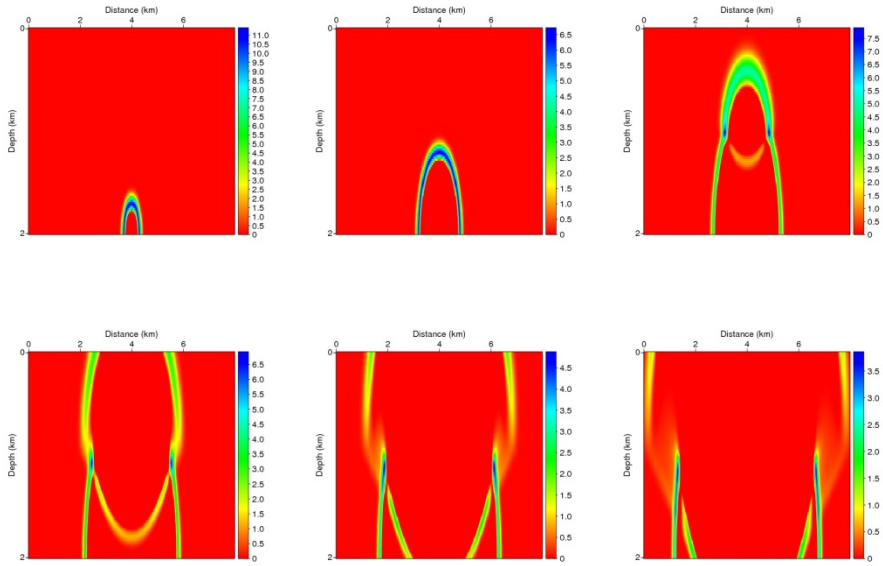


Figure 3. Snapshots of wave motions in the two-dimensional plane.

The source is positioned at a depth of 1.0 km from the boundary. 8.0 km x 2.0 km domain with of interval of 20 m is considered for observing the wave motions. The source wavelet was the first derivative of the Gaussian function. The signal was recorded for 5.0 seconds at an interval of 0.001 second. Each section is at 0.5 second, 1.0 second, 1.5 second, 2.0 second, 2.5 second, and 3.0 second.

Only direct wave is observed for the first time. The reflection wave occurs after the wave reflects from the interface. In particular, a head wave appears in the distance far from the critical distance. To further inspect the critical angle and critical distance, the reflection and transmission energy ratio is plotted in Figure 4.


Figure 4. Energy ratio of the reflection and refraction waves relative to the total energy.

The green and red lines are the energy ratios of the refraction and reflection wave, respectively. When the incident angle is larger than the critical angle of $\pi/6$, the reflection wave contains all the energy from the source. Therefore, if the incident angle is larger than the critical angle, only reflection occurs.

Given the geometry, the critical angle and critical distance can be obtained from Snell's law. Thus, the critical angle is $\pi/6$, and the critical distance is 1.15 km, which corresponds to the computed results shown in Figure 5.

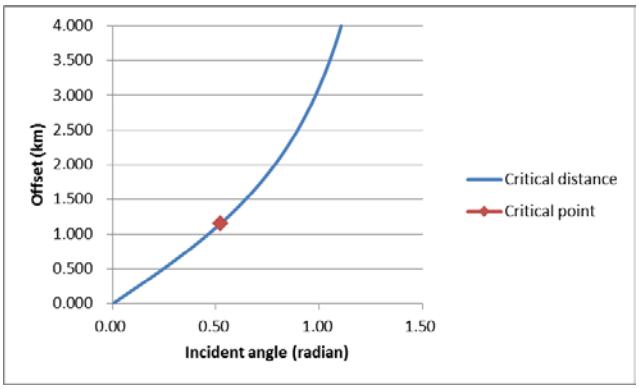


Figure 5. Critical distance at the critical angle under the given circumstances.

To verify the accuracy of the analytic solution, we compared it with the numerical modeling result. Given an identical geometry, numerical finite element modeling was performed in the time-space domain. Figure 6 compares three traces at the receiver positioned 1.0, 2.0, and 3.0 km from the source. There is a big difference between trace from analytic solution and numerical modeling. Thus, each trace is normalized by each maximum value.

(a)

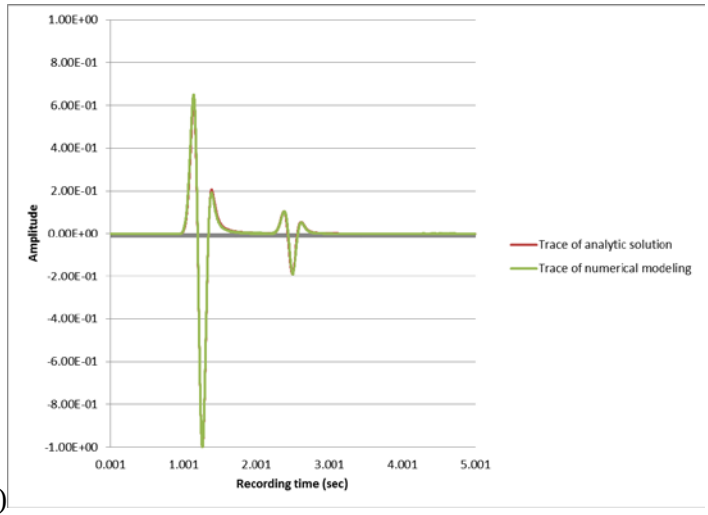


(b)

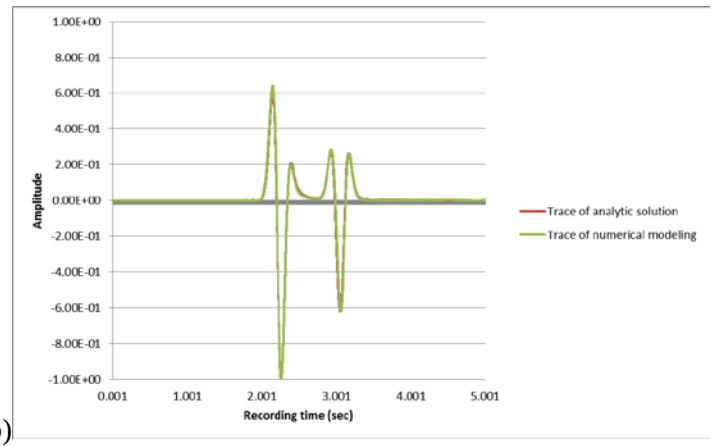


(c)

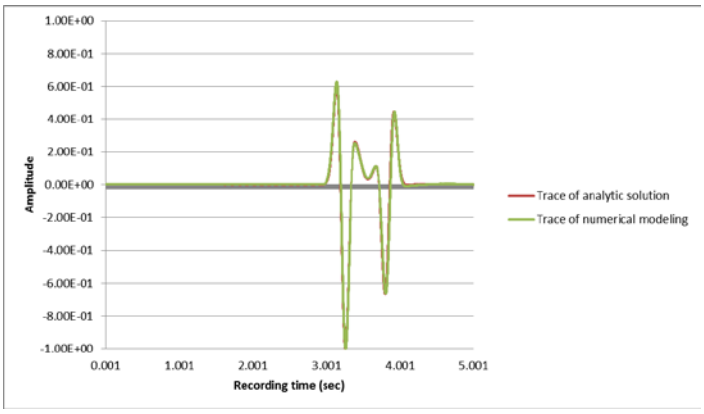


Figure 6. Two traces at the receiver located 1.0 km (a), 2.0 km (b), and 3.0 km (c) from the source. Only negligible error exists between the two traces.

The characteristic of wave events in plane domain is different from that in three-dimensional domain. Thus, we derived each wave event mathematically.

The first integral of $u_1$ and $u_2$, which represents the direct wave, can be easily expressed as

$$\int_{-\infty}^{\infty} \frac{1}{i\beta_1} e^{\pm ikx} e^{-i\beta_1(d-z)} dk = \frac{1}{\sqrt{x^2+(z-d)^2}} e^{-ik_1\sqrt{x^2+(z-d)^2}} \qquad (16)$$

The integral has a direct straight path from the source to a receiver and the decay in wave amplitude is inversely proportional to the square root of the distance. The analytic solution for the reflection wave near the source can be found in many other papers. Hence, we confine the problem to where the offset is larger than the critical distance and the incident angle is larger than the critical angle. The reflection and refraction waves can be derived by performing the complex integral of the second integral of $u_1$ and $u_2$ for a high-speed upper medium.

## 2.3 Evaluation of resultant integral for long ranges

Before performing the contour integration, the second integral term can be written as follows.

Using the property of evenness and oddness of the given function, we obtain

$$u_2 = e^{i\omega t}\phi_2(x,z,\omega) = e^{i\omega t}\int_{-\infty}^{\infty}\frac{1}{i\beta_1}e^{\pm ikx}e^{-i\beta_1(d-z)}dk + e^{i\omega t}\int_{-\infty}^{\infty}\frac{1}{i\beta_1}\left(\frac{\beta_1-b\beta_2}{\beta_1+b\beta_2}\right)e^{\pm ikx}e^{-i\beta_1(d+z)}dk$$

$$\begin{aligned}\varphi_2 &= \int_{-\infty}^{\infty}\frac{1}{i\beta_1}\left(\frac{\beta_1-b\beta_2}{\beta_1+b\beta_2}\right)e^{\pm ikx}e^{-i\beta_1(d+z)}dk \\ &= \int_{-\infty}^{\infty}\{\cos(kx)\pm i\sin(kx)\}\frac{1}{i\beta_1}\left(\frac{\beta_1-b\beta_2}{\beta_1+b\beta_2}\right)e^{-i\beta_1(d+z)}dk \\ &= 2\int_0^{\infty}\cos(kx)\frac{1}{i\beta_1}\left(\frac{\beta_1-b\beta_2}{\beta_1+b\beta_2}\right)e^{-i\beta_1(d+z)}dk \\ &(\because \textit{evenness and oddness in terms of } k) \\ &= 2\int_0^{\infty}\frac{e^{ikx}+e^{-ikx}}{2}\frac{1}{i\beta_1}\left(\frac{\beta_1-b\beta_2}{\beta_1+b\beta_2}\right)e^{-i\beta_1(d+z)}dk \\ &(\because \cos kx = \frac{e^{ikx}+e^{-ikx}}{2}) \\ &= \int_0^{\infty}\left(e^{ikx}+e^{-ikx}\right)\frac{1}{i\beta_1}\left(\frac{\beta_1-b\beta_2}{\beta_1+b\beta_2}\right)e^{-i\beta_1(d+z)}dk\end{aligned} \tag{17}$$

Now, let us perform the contour integration to theoretically evaluate these seismic events. There are no poles, but two branch points in the given integral (See Appendix A). Thus, like Pekeris, Officer, and Ewing, we take the branch lines as shown in Figure 7 (Pekeris, 1948; Officer, 1958; Ewing et al, 1957)

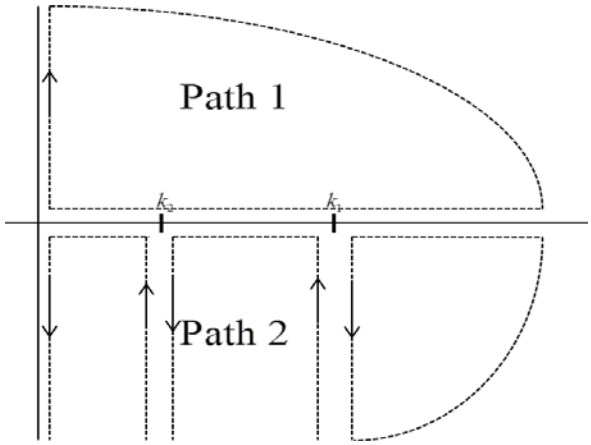


Figure 7. : Path of contour integration for the second integral of $u_1$ and $u_2$

The path of contour integration is identical to that of Pekeris. To avoid the branch points, the path is set as above. Path 1 remains only in the first quadrant and Path 2 remains only in the fourth quadrant. Thus, neither of paths crosses the branch points. $e^{ikx}$ is taken as an infinite term in the first quadrant and $e^{-ikx}$ is taken as an infinite term in the fourth quadrant to satisfy the problem condition.

Path 1:

$$\int_0^{\infty} e^{ikx}\frac{1}{i\beta_1}\left(\frac{\beta_1-b\beta_2}{\beta_1+b\beta_2}\right)e^{-i\beta_1(d+z)}dk=\int_0^{i\infty} e^{ikx}\frac{1}{i\beta_1}\left(\frac{\beta_1-b\beta_2}{\beta_1+b\beta_2}\right)e^{-i\beta_1(d+z)}dk+\lim_{k\to\infty}\int_{i\infty}^{0} e^{ikx}\frac{1}{i\beta_1}\left(\frac{\beta_1-b\beta_2}{\beta_1+b\beta_2}\right)e^{-i\beta_1(d+z)}dk \tag{18}$$

Path 2:

$$\begin{aligned}\int_0^{\infty} e^{-ikx}\frac{1}{i\beta_1}\left(\frac{\beta_1-b\beta_2}{\beta_1+b\beta_2}\right)e^{-i\beta_1(d+z)}dk=&\int_0^{-i\infty} e^{-ikx}\frac{1}{i\beta_1}\left(\frac{\beta_1-b\beta_2}{\beta_1+b\beta_2}\right)e^{-i\beta_1(d+z)}dk\\&+\lim_{k\to\infty}\int_{-i\infty}^{0} e^{ikx}\frac{1}{i\beta_1}\left(\frac{\beta_1-b\beta_2}{\beta_1+b\beta_2}\right)e^{-i\beta_1(d+z)}dk\\&+\int_{k_1}^{-i\infty} e^{-ikx}\frac{1}{i\beta_1}\left(\frac{\beta_1-b\beta_2}{\beta_1+b\beta_2}\right)e^{-i\beta_1(d+z)}dk\\&+\int_{-i\infty}^{k_1} e^{-ikx}\frac{1}{i\beta_1}\left(\frac{\beta_1-b\beta_2}{\beta_1+b\beta_2}\right)e^{-i\beta_1(d+z)}dk\\&+\int_{k_2}^{-i\infty} e^{-ikx}\frac{1}{i\beta_1}\left(\frac{\beta_1-b\beta_2}{\beta_1+b\beta_2}\right)e^{-i\beta_1(d+z)}dk\\&+\int_{-i\infty}^{k_2} e^{-ikx}\frac{1}{i\beta_1}\left(\frac{\beta_1-b\beta_2}{\beta_1+b\beta_2}\right)e^{-i\beta_1(d+z)}dk\end{aligned} \tag{19}$$

The original term is the sum of the integrals of path 1 and 2. The first integrals of path 1 and 2 cancel each other out. The second integrals of path 1 and 2 vanish at $\infty$ in the first and fourth quadrants, respectively. Consequently, the reflection wave and head wave can be derived from the

four left integrals. Two integrands in terms of $k_1$ of the four left integrals imply the reflection wave, and the other two in terms of $k_2$ represent the head wave. Thus, we have

$$\int_{k_1}^{-i\infty} e^{-ikx}\frac{1}{i\beta_1}\left(\frac{\beta_1-b\beta_2}{\beta_1+b\beta_2}\right)e^{-i\beta_1(d+z)}dk+\int_{-i\infty}^{k_1} e^{-ikx}\frac{1}{i\beta_1}\left(\frac{\beta_1-b\beta_2}{\beta_1+b\beta_2}\right)e^{-i\beta_1(d+z)}dk$$
$$+\int_{k_2}^{-i\infty} e^{-ikx}\frac{1}{i\beta_1}\left(\frac{\beta_1-b\beta_2}{\beta_1+b\beta_2}\right)e^{-i\beta_1(d+z)}dk+\int_{-i\infty}^{k_2} e^{-ikx}\frac{1}{i\beta_1}\left(\frac{\beta_1-b\beta_2}{\beta_1+b\beta_2}\right)e^{-i\beta_1(d+z)}dk$$
$$=\int_{k_1,-i\infty}^{k_1} e^{-ikx}\left[F(\beta_1,\beta_2)-F(-\beta_1,\beta_2)\right]dk+\int_{k_2,-i\infty}^{k_2} e^{-ikx}\left[F(\beta_1,\beta_2)-F(\beta_1,-\beta_2)\right]dk \tag{20}$$

$$where\quad F(\beta_1,\beta_2)=\frac{1}{i\beta_1}\left(\frac{\beta_1-b\beta_2}{\beta_1+b\beta_2}\right)e^{-i\beta_1(z+d)}$$

The integrands involving exponential function diverge to zero when the imaginary part of $k$ is large negative. Thus, only the value near real axis is considered for contour integration.

### 2.3.1 Evaluation of reflection wave

First, let us evaluate the reflection wave. The integrand in terms of $k_1$ is

$$\varphi_{k_1} = \int_{k_1,-i\infty}^{k_1} e^{-ikx}\left[F(\beta_1,\beta_2) - F(-\beta_1,\beta_2)\right]dk \tag{21}$$

Because $x$ is sufficiently larger than the critical distance, let us consider the small imaginary part of $k$ near a branch point $k_1$.

$$k = k_1\lambda \qquad where\ \lambda = 1 - iu \tag{22}$$

Then, for a small value of $u$, we have

$$k = k_1\lambda \approx k_1$$
$$dk = -ik_1 du$$
$$\beta_1 = \sqrt{k_1^2 - k^2} = \sqrt{k_1^2 - k_1^2\lambda^2} = k_1\sqrt{1-\lambda^2} \approx k_1\sqrt{2iu} = k_1\sqrt{2u}e^{i(\pi/4)}$$
$$\beta_2 = \sqrt{k_2^2 - k^2} = k_1\sqrt{\frac{c_1^2}{c_2^2} - \lambda^2} \approx k_1\sqrt{\frac{c_1^2}{c_2^2} - 1} \approx ik_1\sqrt{1 - \frac{c_1^2}{c_2^2}} = ik_1\mu$$
$$where \quad \mu = \sqrt{1 - \frac{c_1^2}{c_2^2}}$$
$$F(\beta_1,\beta_2) - F(-\beta_1,\beta_2) = \frac{1}{i\beta_1}\left(\frac{\beta_1 - b\beta_2}{\beta_1 + b\beta_2}\right)e^{-i\beta_1(z+d)} - \frac{1}{-i\beta_1}\left(\frac{-\beta_1 - b\beta_2}{-\beta_1 + b\beta_2}\right)e^{i\beta_1(z+d)}$$
$$= \frac{2}{i\beta_1}\left\{\frac{\left(\beta_1^2 + b^2\beta_2^2\right)\cos\left[\beta_1\left(z+d\right)\right] + 2ib\beta_1\beta_2\sin\left[\beta_1\left(z+d\right)\right]}{\beta_1^2 - b^2\beta_2^2}\right\}$$
$$\approx \frac{-2e^{-i(\pi/4)}}{ik_1\sqrt{2u}}\left\{\cos(m\sqrt{u}) + \frac{2\sqrt{2x}e^{i(\pi/4)}}{b\mu}\sin\left(m\sqrt{u}\right)\right\}$$
$$where \quad m = \sqrt{2}k_1e^{i(\pi/4)}(z+d) \tag{23}$$

Substituting the variable which is parameterized with $k_1$ into $\varphi_{k_1}$, $\varphi_{k_1}$ becomes

$$\begin{aligned}\varphi_{k_1} &= \int_{\infty}^{0} e^{-ikx}\frac{-2e^{-i(\pi/4)}}{ik_1\sqrt{2u}}\left[\cos(m\sqrt{u})+\frac{2\sqrt{2u}e^{i(\pi/4)}}{b\mu}\sin(m\sqrt{u})\right](-ik_1du)\\ &= \int_{\infty}^{0} e^{-ikx}\frac{-2e^{-i(\pi/4)}}{ik_1\sqrt{2u}}\cos(m\sqrt{u})(-ik_1du)\\ &\qquad + \int_{\infty}^{0} e^{-ikx}\frac{-2e^{-i(\pi/4)}}{ik_1\sqrt{2u}}\frac{2\sqrt{2u}e^{i(\pi/4)}}{b\mu}\sin(m\sqrt{u})(-ik_1du)\\ &= \int_{0}^{\infty} e^{-ikx}\frac{-2e^{-i(\pi/4)}}{\sqrt{2u}}\cos(m\sqrt{u})(du)-\int_{0}^{\infty} e^{-ikx}\frac{4}{b\mu}\sin(m\sqrt{u})(du)\end{aligned} \tag{24}$$

Because $e^{-ikx}=e^{-ik_1(1-iu)x}=e^{-ik_1x}e^{-k_1xu}$, equation (24) can be written as

$$\varphi_{k_1}=\int_{0}^{\infty} e^{-ik_1x}e^{-k_1xu}\frac{-2e^{-i(\pi/4)}}{\sqrt{2u}}\cos(m\sqrt{u})(du)-\int_{0}^{\infty} e^{-ik_1x}e^{-k_1xu}\frac{4}{b\mu}\sin(m\sqrt{u})(du)$$

Let us change a variable of integration to $v$, where $u=v^2$. Then, we have

$$\begin{aligned}\varphi_{k_1} &= -2\sqrt{2}e^{-i(\pi/4)}e^{-ik_1x}\int_{0}^{\infty} e^{-k_1xv^2}\cos(mv)dv-\frac{8}{b\mu}e^{-ik_1x}\int_{0}^{\infty} e^{-k_1xv^2}\sin(mv)dv\\ &= -2\sqrt{2}e^{-i(\pi/4)}e^{-ik_1x}\frac{\sqrt{\pi}e^{-\frac{m^2}{4k_1x}}}{2\sqrt{k_1x}}-\frac{8}{b\mu}e^{-ik_1x}\frac{m}{2k_1x}\frac{\sqrt{\pi}e^{-\frac{m^2}{4k_1x}}}{2\sqrt{k_1x}}\\ &= -\frac{\sqrt{2\pi}e^{-i(\pi/4)}}{\sqrt{k_1x}}e^{-ik_1x}e^{-\frac{m^2}{4k_1x}}-\frac{2m\sqrt{\pi}}{b\mu k_1x\sqrt{k_1x}}e^{-ik_1x}e^{-\frac{m^2}{4k_1x}}\end{aligned} \tag{25}$$

Now, we have

$$\varphi_{k_1} = e^{-ik_1 x} e^{-\frac{m^2}{4k_1 x}} \frac{\sqrt{\pi}}{\sqrt{k_1 x}} \left[ \sqrt{2} e^{-i(\pi/4)} + \frac{2m}{b\mu k_1 x} \right] \tag{26}$$

Assuming that $x$ is sufficiently large, the term with $1/x$ is negligible.

Thus, the approximated solution is

$$\varphi_{k_1} = e^{-ik_1 x} e^{-\frac{m^2}{4k_1 x}} \frac{\sqrt{2\pi} e^{-i(\pi/4)}}{\sqrt{k_1 x}} = \frac{\sqrt{2\pi i}}{\sqrt{k_1 x}} e^{-ik_1 \left( x + \frac{(z+d)^2}{2x} \right)} \tag{27}$$

With the first two terms of the series expansion, the exponential term is expressed as

$$\sqrt{x^2 + (z+d)^2} = x \left[ 1 + \frac{(z+d)^2}{x^2} \right]^{1/2} = x \left[ 1 + \frac{(z+d)^2}{2x^2} \right]^{1/2} \tag{28}$$

Consequently,

$$\varphi_{k_1} = \frac{\sqrt{2\pi i}}{\sqrt{k_1 x}} e^{-ik_1 (x^2 + (z+d)^2)^{1/2}} \tag{29}$$

The exponential term shows the reflection ray path from Snell's law. A phase change of $\pi$ occurs in the equation. The amplitude of the reflection wave in the two-dimensional plane domain is proportional to the inverse of the square root of the distance between the source and the receiver. To verify this fact, we performed a regression analysis. Although we should pick up certain amplitude points on the reflection event, the wave amplitude varied for a few milliseconds at each receiver. Thus, we selected the strongest signal at each receiver. Then, random receiver points were selected and we attempted to fit them to a polynomial of $1/\sqrt{x}$. Figure 8 shows the result.

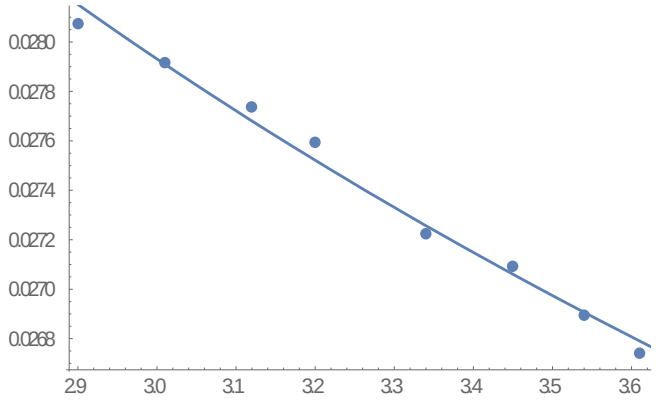


Figure 8. : Polynomial fitting of the amplitude point of the reflection wave to the function of $1/\sqrt{x}$ .

The amplitude points on the reflection events are well-fitted to the given polynomial function. The receivers were randomly selected to check the amplitude pattern to distance $x$. Then, 8 random points were selected as a sample and we used the regression analysis module of Mathematica to perform the regression analysis. These results are well-fitted to the function of $1/\sqrt{x}$ , and the coefficient of determination is 0.985.

Furthermore, the amplitude of the reflection wave is related to the angular frequency $\omega$. Although the amplitude of the analytic solution in three dimensions is independent of $\omega$ (Pekeris, 1948), the amplitude in two dimensions is proportional to the inverse of the square root of $\omega$. To verify this trend, we recorded the angular frequency spectrum of the reflection wave at a receiver, and attempted to fit it to a polynomial of $1/\sqrt{\omega}$. Figure 9 shows the relationship between the amplitude and $\omega$.

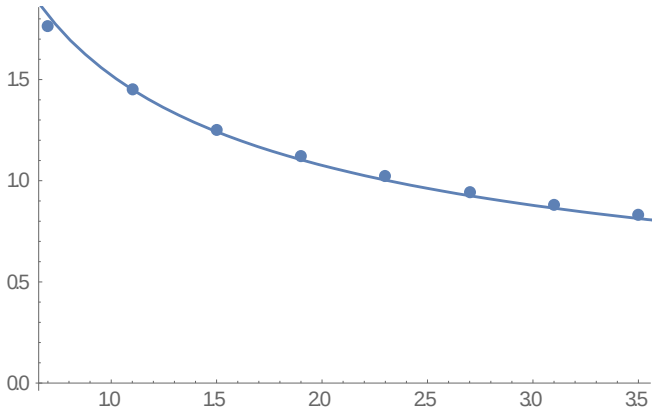


Figure 9. : Polynomial fitting of the angular frequency spectrum to the function of $1/\sqrt{\omega}$.

The receiver 1.5 km from the source was selected for a regression analysis. The spectrum was recorded from 0.7 Hz to 3.5 Hz at an interval of 0.4 Hz. The results are well-fitted to the function of $1/\sqrt{\omega}$, and the coefficient of determination is 0.998.

### 2.3.2 Evaluation of refraction wave

By performing the contour integration in terms of $k_2$, the head wave can be invented. The integrand in terms of $k_2$ is

$$\varphi_{k_2} = \int_{k_2,-i\infty}^{k_2} e^{-ikx}\left[F(\beta_1,\beta_2) - F(\beta_1,-\beta_2)\right]dk \tag{30}$$

Using the previous procedure for $\varphi_{k_1}$, let us assume

$$k = k_1\eta \qquad where\ \ \eta = \frac{c_1}{c_2} - iu \tag{31}$$

Then, for a small value of $u$, we have

$$k = k_1\eta \approx k_1\frac{c_1}{c_2} = k_2$$

$$dk = -ik_1 du$$

$$\beta_1 = \sqrt{k_1^2 - k^2} = k_1\sqrt{1-\eta^2} \approx k_1\left(1-\frac{c_1^2}{c_2^2}\right)^{1/2} = k_1\mu$$

$$\beta_2 = \sqrt{k_2^2 - k^2} = k_1\left(\frac{c_1^2}{c_2^2} - \eta^2\right)^{1/2} \approx k_1\left(2iu\frac{c_1}{c_2}\right)^{1/2}$$

$$F(\beta_1,\beta_2) - F(\beta_1,-\beta_2) = \frac{1}{i\beta_1}\left(\frac{\beta_1 - b\beta_2}{\beta_1 + b\beta_2}\right)e^{-i\beta_1(z+d)} - \frac{1}{i\beta_1}\left(\frac{\beta_1 + b\beta_2}{\beta_1 - b\beta_2}\right)e^{-i\beta_1(z+d)}$$

$$= \frac{4ib\beta_2}{\beta_1^2 - b^2\beta_2^2}e^{-i\beta_1(z+d)}$$

$$\approx \frac{4ib\sqrt{2iu(c_1/c_2)}}{k_1\mu^2}e^{-ik_1\mu(z+d)} \tag{32}$$

Substituting the variable that was parameterized with $k_2$ into $\varphi_{k_2}$, $\varphi_{k_2}$ becomes

$$\begin{aligned}\varphi_{k_2} &= \int_{\infty}^{0} e^{-ikx}\frac{4ib(2uc_1/c_2)^{1/2}e^{i(\pi/4)}}{k_1\mu^2}e^{-ik_1\mu(z+d)}(-ik_1du)\\ &= -\frac{4\sqrt{2}b(c_1/c_2)^{1/2}e^{i(\pi/4)}}{k_1\mu^2}e^{-ik_1\mu(z+d)}\int_0^{\infty}e^{-iku}\sqrt{u}du\end{aligned} \tag{33}$$

Because $e^{-ikx} = e^{-ik_1(\frac{c_1}{c_2}-iu)x} = e^{-ik_2x}e^{-k_1xu}$, equation (33) can be rewritten as

$$\begin{aligned}\varphi_{k_2} &= -\frac{4\sqrt{2}b(c_1/c_2)^{1/2}}{\mu^2}e^{-ik_1\mu(z+d)}e^{-ik_2x}\int_0^{\infty}e^{-k_1xu}\sqrt{u}du\\ &= -\frac{4\sqrt{2}b(c_1/c_2)^{1/2}}{\mu^2}e^{-ik_1\mu(z+d)}e^{-ik_2x}\left[\frac{\sqrt{\pi}}{2(k_1x)^{3/2}}\right]\\ &= -\frac{2\sqrt{2}b(c_1/c_2)^{1/2}}{\mu^2}\frac{\sqrt{\pi}}{(k_1x)^{3/2}}e^{-i(k_2x+k_1\mu(z+d))}\end{aligned} \tag{34}$$

Consequently,

$$\begin{aligned}\varphi_{k_2} &= -\frac{2\sqrt{2\pi}b\sqrt{k_1c_1/c_2}}{\mu^2(k_1x)^{3/2}}e^{-i(k_2x+k_1\mu(z+d))}\\ &= -\frac{2\sqrt{2\pi}b\sqrt{k_2}}{\mu^2k_1^2x^{3/2}}e^{-i(k_2x+k_1\mu(z+d))}\end{aligned} \tag{35}$$

Unlike the direct and reflection waves, the head wave includes a $k_2$ term. The exponential term, which implies the travel time of wave, has both $k_1$ and $k_2$. Thus, some part of the path propagates with velocity $c_1$, and the other part propagates with velocity $c_2$. From the work of Pekeris, who rewrote the exponent term with the critical angle (Pekeris, 1948), we can know that the wave enters at the critical angle and reflects out at the critical

angle.

$$
\begin{aligned}
k_2 r + k_1 \mu (z+d) &= \omega \left[ \frac{x}{c_2} + \frac{z+d}{c_1} \left( 1 - \frac{c_1^2}{c_2^2} \right)^{1/2} \right] \\
&= \omega \left[ \frac{x}{c_2} + \frac{z+d}{c_1} \cos\theta_c \right] \\
&= \omega \left[ \frac{x-(z+d)\tan\theta_c}{c_2} + \frac{z+d}{c_1} \left( \cos\theta_c + \frac{c_1}{c_2} \tan\theta_c \right) \right] \\
&= \omega \left[ \frac{x-(z+d)\tan\theta_c}{c_2} + \frac{z+d}{c_1} \left( \frac{\cos^2\theta_c + \sin^2\theta_c}{\cos\theta_c} \right) \right] \\
&= \omega \left[ \frac{x-(z+d)\tan\theta_c}{c_2} + \frac{(z+d)/\cos\theta_c}{c_1} \right]
\end{aligned}
\tag{36}
$$

Additionally, the amplitude of the head wave in the two-dimensional plane domain is proportional to the inverse of $x^{3/2}$, where the distance is $x$. As previously implemented, the amplitude points were selected as a sample for a regression analysis. Figure 10 shows the results of fitting to the polynomial of $1/x^{3/2}$.

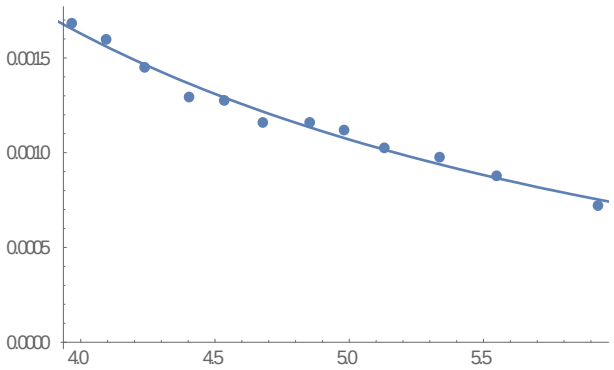


Figure 10. : Polynomial fitting of the amplitude point of the head wave to the function of $1/x^{3/2}$.

The strongest signal of the refraction event was selected to implement a regression analysis. The receivers were randomly selected to check the amplitude pattern to distance $x$. Then, 12 random points were selected as a sample and we used a regression analysis module in the Mathematica program to perform the analysis. The results are well-fitted to the function of $1/x^{3/2}$, and the coefficient of determination is 0.982.

In addition, the amplitude of the head wave is related to the angular frequency $\omega$. Although the amplitude of the analytic solution in three dimensions is proportional to the inverse of $\omega$ (Pekeris, 1948), the amplitude in two dimensions is proportional to the inverse of $\omega^{3/2}$. To verify this trend, we recorded the angular frequency spectrum of the head wave at a receiver, and attempted to fit it to a polynomial of $1/\omega^{3/2}$. Figure 11 shows the relationship between the amplitude and $\omega$.

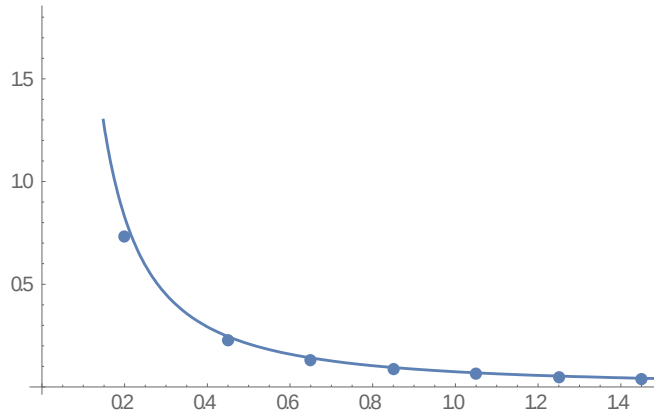


Figure 11. : Polynomial fitting of the amplitude point of the head wave to the function of $1/\omega^{3/2}$.

The receiver 1.5 km from the source was selected for a regression analysis. The spectrum was recorded from 0.05 Hz to 1.5 Hz at an interval of 0.25 Hz. These results are well-fitted to the function of $1/\omega^{3/2}$ and the coefficient of determination is 0.923.

We also attached table 1 to compare the two-dimensional and three-dimensional solutions.

| | 2D solution | 3D solution |
|---|---|---|
| **Reflection wave** | | |
| Term of integrand | Exponential function | Hankel function |
| Relation between amplitude and distance $(x)$ | $Amp \propto 1/\sqrt{x}$ | $Amp \propto 1/x$ |
| Relation between amplitude and angular frequency $(\omega)$ | $Amp \propto 1/\sqrt{\omega}$ | Independent |
| **Head wave** | | |
| Term of integrand | Exponential function | Hankel function |
| Relation between amplitude and distance $(x)$ | $Amp \propto 1/x\sqrt{x}$ | $Amp \propto 1/x^2$ |
| Relation between amplitude and angular frequency $(\omega)$ | $Amp \propto 1/\omega\sqrt{\omega}$ | $Amp \propto 1/\omega$ |

Table 1. Comparison between the two-dimensional and three-dimensional solutions.

# Chapter 3 Conclusion

In this paper, we theoretically solve the problem of acoustic wave propagation in two-dimensional unbounded plane media. Unlike the three-dimensional solution with the Hankel function, which results in difficult numerical integration, the two-dimensional solution with an exponential function can be inverted with the two-dimensional inverse Fourier transform to obtain wave motion in the time-space domain. Furthermore, we visualized the wave propagation in a given geometry using computational arithmetic to allow more intuitive understanding of wave behavior. After a simple operation, we found that the amplitude of the reflection wave in the two-dimensional plane is proportional to the inverse of the square root of the distance and angular frequency, and that of the head wave is proportional to the inverse of the square root of the cube of the distance and angular frequency. With the knowledge from this study, calculation of acoustic wave propagation in a two-dimensional bounded plane medium is feasible.

# Chapter 4 References

Brekhovskikh L. M., and Lysanov Y. P., 1991, Fundamentals of ocean acoustics, 1st edition: Springer.

Buckingham M. J., 1992, Ocean-acoustic propagation models: J. Acoustique.

DeSanto J. A., 1992, Scalar wave theory: Springer.

Dovrin M. B., 1952, Introduction to geophysical prospecting, 1st edition: McGraw-Hill.

Etter P. C., 2013, Underwater acoustic modeling and simulation, 4th edition: CRC press.

Ewing M. B., Jardetzky W. S., and Press F., 1958, Elastic waves in layered media: McGraw Hill.

Jensen F. B., Kuperman W. A., Porter M. B., and Schmidt H., 1997, Computational ocean acoustics, 1st edition: Springer.

Katsnelson B. G. and Prtnikov V. G., 2002, Shallow water acoustics: Springer.

Kennett B., 1983, Seismic wave propagation in stratified media, 1st edition: ANU E press.

Lurton X., 2002, An introduction to underwater acoustics: principles and applications: Springer-Praxis.

Officer C. B., 1958, Introduction to the theory of sound transmission with application in the ocean: McGraw Hill.

Pekeris C. L., 1948, Theory of propagation of explosive source in shallow water: The Geological Society of America Memoir 27.

Pilant W. L., 2012, Elastic waves in the earth: Elsevier.

Pujol J., 2003, Elastic wave propagation and generation in seismology: Cambridge.

Yilmaz O., 2001, Seismic data analysis, 2nd edition: Society of Exploration Geophysicists.

# 초 록

1948년 C.L. Pekeris는 음향 매질 내 파동 전파 이론의 기틀을 마련하였다. 이후로, 음향 매질 내 파동 전파 이론은 지구물리학, 해양학을 비롯한 파동 전파 현상을 다루는 모든 기초 학문의 필수적인 내용으로 자리잡았다. 실제로 그는 원통 좌표계를 도입하여 음향 반무한 매질 내에서의 파의 거동을 수학적으로 풀어냈다. 그가 구한 음향 반무한 매질 내에서의 해는 수학적으로 완벽하나, 베셀 함수와 한켈 함수를 포함하여 이를 컴퓨터 프로그래밍을 통한 수치적 재현에는 많은 어려움이 따른다. 따라서, 3차원 원통 좌표계 대신 2차원 평면 좌표계에 적용하여 이론 해를 다시 도출한다면, 음향 반무한 매질 내에서의 해는 훨씬 간단히 표현 될 수 있다. 따라서, 2차원 평면 내에서의 해를 컴퓨터 프로그래밍을 통해 보다 쉽게 재현 할 수 있고, 이는 파동 전파 이론을 공부하는 학생들에게 큰 도움이 될 것이다. 본 논문에서는 2차원 평면 상에서의 음향 반무한 매질 내 해를 도출하였고, 이를 수치적 모델링 결과와 비교하였으며, 회귀분석을 통해 구한 결과를 검증하였다.

**주요어** : 파동전파이론, 반무한, 음향 매질, 2차원 평면, 복소적분

**학번 : 2014-20528**

공학석사 학위논문

# Acoustic wave propagation in Two-dimensional unbounded layered media

## 무한 2층 평면매질 내에서의 음향 파동 전파 이론

**2016년 2 월**

서울대학교 대학원

에너지시스템공학부

김 장 우

# Abstract

Since Pekeris established the theory of wave propagation in acoustic media in 1948, the theory has been crucial in understanding the phenomena of acoustic wave propagation for beginners in geophysics and oceanography. Pekeris theoretically solved the acoustic wave motion problem of unbounded two layers in axially symmetric cylindrical coordinate system. Although his work is mathematically impeccable, his solution is somewhat complicated because it includes a Bessel function, which makes it difficult to calculate numerically. A much simpler solution can be obtained by introducing a two-dimensional plane domain instead of a three-dimensional cylindrical environment. This attempt enables beginners to more intuitively comprehend the characteristics of wave motion in acoustic media and to visualize the wave propagation in acoustic media through modern computer programming. To verify the accuracy of the newly derived two-dimensional solution, the analytical and numerical results are compared, and a regression analysis is performed.

**Keywords : Wave propagation, Unbounded, Acoustic media, Two-dimensional, Contour integration**

**Student Number : 2014-20528**

# Contents

# List of Figures

# List of Tables

# Chapter 1 Introduction

## 1.1 Historical background

The theory of wave propagation in acoustic or elastic media is a foundation for understanding of the behavior of a wave. Even in a complicated seismic section, many seismic events can be interpreted using the concepts of this theory. Thus, beginners in geophysics and oceanography should be familiar with the theory. Pekeris initially established this theory in 1948 by obtaining a normal-mode solution (Pekeris, 1948). He derived a solution in two unbounded media with an explosive point source in an axial symmetrical cylindrical coordinate and compared the findings with experimental results. In 1950, Press and Ewing extended the concepts of this theory to elastic media, and drove a solution in the elastic media and two-layered acoustic-elastic coupled media (Ewing and Press, 1950). Officer treated the acoustic wave propagation theory in his book “Introduction to the Theory of sound transmission with application in the ocean” in 1958, which included a discussion of Pekeris’ work (Officer, 1958). Following Ewing and Officer, Dobrin introduced this theory in his book “Introduction to geophysical prospecting” (Dobrin, 1952), Brekhovskikh and Lurton explained it in their fundamental books for beginners in geophysics (Brekhovskikh, 1991; Lurton, 2002), and Kennett extended the idea to stratified media (Kennett, 1983). Yilmaz mentioned this concept for seismic data analysis (Yilmaz, 2001), and efforts in computational and numerical acoustics with this idea can be found in the books of Jensen and Etter (Jensen, 1997; Etter, 2013). Furthermore, this key theory has been included in many other classic books and papers in geophysics and oceanography as a fundamental concept for wave propagation (DeSanto, 1992; Buckingham, 1992; Katsnelson, 2002; Pujol, 2003; Pilant, 2012).

## 1.2 Purpose

To intuitively comprehend the wave propagation characteristics in acoustic media, visualizing the wave motion of the analytic solution using modern computer programming is particularly useful. Beginners more readily accept these concepts via visualizing the phenomena of wave propagation than by relying solely on mathematical conclusions. The solution obtained from Pekeris' theory is perfect in mathematical terms, but it is complicated and difficult to reproduce the wave motion through numerical calculation. In addition, the two-dimensional approximation solution is utilized for verification of numerical modeling technique because it is difficult to calculate the three-dimensional solution using computer arithmetic. Thus, we focused on the two-dimensional plane domain instead of the three-dimensional solution to simplify the solution and reproduce the wave motion using numerical computations. For the two-dimensional wave equation, a complex Hankel function can be replaced with an exponential function. This substitution makes a seismogram far easier to compute in the time-space domain by taking only two-dimensional Fourier transforms. The solution in frequency-wavenumber is enough to generate the seismogram. Thus, we finished our derivation to obtain the solution in frequency-wavenumber domain.

## 1.3 Application

We also generated the snapshots to easily observe the wave front of each wave event. It is possible to understand of propagation aspects of each wave through the snapshot section. We only deal with the unbounded case in this study, but it can be extended to the problem of bounded case. In bounded problem, there is a normal mode reflection which is reflected to the boundary of the media several times. After deriving the solution of bounded problem, it is possible to simulate the seismic signals under the shallow marine environment. However, the simplicity of the solution makes it difficult to reflect a complex actual physical environment. Above this, this study can be a foundation to the theory of acoustic-elastic coupled and elastic media. Acoustic media is considered for the simplicity of discussion. But there exist elastic effects of ocean bottom layer. Therefore, acoustic-elastic solution can give a much exact model for the ocean system.

In this paper, we used the identical procedures as Pekeris and focused on visualizing the phenomena of wave propagation using computer arithmetic by confining the domain to a two-dimensional plane instead of a three-dimensional cube. To verify the new solution, we compare the results to those of a numerical finite element modeling technique using a least square fitting.

# Chapter 2 Theory

## 2.1 Fundamental solution for the wave equation in the two-dimensional plane domain

The wave equation in a two-dimensional plane domain (x-z) is

$$\nabla^2 u = \frac{\partial^2 u}{\partial x^2} + \frac{\partial^2 u}{\partial z^2} = \frac{1}{c^2}\frac{\partial^2 u}{\partial t^2} \tag{1}$$

where $u$ is the velocity potential. To solve a given problem, we can take a product solution of the equation,

$$u = e^{i\omega t} F(x) G(z) \tag{2}$$

We will consider a simple harmonic point source with a single frequency $\omega$.

Substituting a product solution into equation (1) yields

$$\nabla^2 u = e^{i\omega t}\frac{d^2 F(x)}{dx^2} G(\mathrm{z}) + e^{i\omega t} F(x)\frac{d^2 G(z)}{dz^2} = -\frac{\omega^2}{c^2} e^{i\omega t} F(x) G(z) \tag{3}$$

After a simple reduction, we obtain

$$\frac{d^2 F(x)}{dx^2}\frac{1}{F(x)} = -\frac{d^2 \mathrm{G(z)}}{dz^2}\frac{1}{\mathrm{G(z)}} - \frac{\omega^2}{c^2} \tag{4}$$

The left side of equation (4) is independent of $z$, and the right side of equation (4) is independent of $x$. To satisfy the equality of each side for any value of $x$ and $z$, equation (4) on each side must be equal to a constant $-k^2$. Thus, we have

$$\frac{d^2F(x)}{dx^2} + k^2F(x) = 0$$
$$\frac{d^2G(z)}{dz^2} + \left(\frac{\omega^2}{c^2} - k^2\right)G(z) = 0 \tag{5}$$

The fundamental solution of $F(x)$ and $G(z)$ can be represented as

$$F(x) = e^{\pm ikx}$$
$$G(z) = e^{\pm i\beta z} \quad \text{where} \quad \beta = \left(\frac{\omega^2}{c^2} - k^2\right)^{1/2} \tag{6}$$

Finally, the velocity potential $u$ can be expressed as

$$u = F(x)G(z)e^{i\omega t} = e^{\pm ikx}e^{\pm i\beta z}e^{i\omega t} \tag{7}$$

## 2.2 Physical solution for the wave equation in the two-dimensional plane domain

Now, let us consider the following physical domain. The physical properties of the acoustic media for the wave propagation problem to be solved are shown in Figure 1 (Pekeris, 1948).

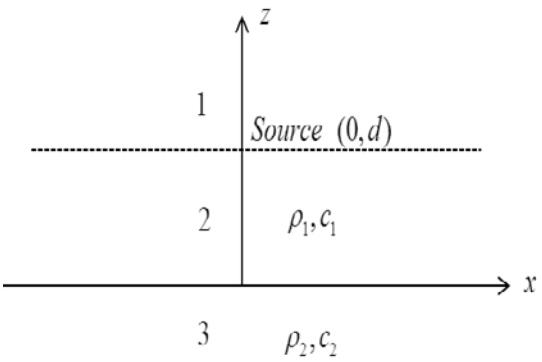


Figure 1. This is the physical properties of the acoustic media for the wave propagation problem to be solved are shown in Figure 1 (Pekeris, 1948).

A point source exists at $x = 0, z = d$. There is a plane boundary at $z = 0$ between two media of velocities $c_1$ and $c_2$ and densities $\rho_1$ and $\rho_2$, respectively. The fundamental solution of the wave equation in the two-dimensional domain is

$$u = F(x)G(z)e^{i\omega t} = G(z)e^{\pm ikx}e^{i\omega t} \tag{8}$$

The form of $G(z)$ for each area of Figure 1 is

$$
\begin{aligned}
G_1 &= Ae^{-i\beta_1 z} + Ee^{i\beta_1 z} \qquad z > d \\
G_2 &= Be^{-i\beta_1 z} + Ce^{i\beta_1 z} \qquad 0 \le z \le d \\
G_3 &= De^{i\beta_2 z} + Fe^{-i\beta_2 z} \qquad z < 0
\end{aligned} \tag{9}
$$

where $\beta_1 = \sqrt{\frac{\omega^2}{c_1^2} - k^2} = \sqrt{k_1^2 - k^2}$, $\beta_2 = \sqrt{\frac{\omega^2}{c_2^2} - k^2} = \sqrt{k_2^2 - k^2}$.

where the subscript number of $G(z)$ indicates each area in Figure 1.

Constant $E$ should be zero to avoid the unreasonable physical condition of an exponential increase of $G_1$ with positive $z$. With an identical approach, $F$ should be zero to avoid blowing up of $G_3$ with negative $z$.

To ensure that there are outgoing waves from the point source and satisfy the boundary condition between two media, the value of $\beta(\beta_1, \beta_2)$ should be determined to be either positive real or negative imaginary, depending on the value of $k$.

Our solution must comply with boundary condition at the interface between two media and near the source. The continuity of pressure and vertical particle velocity should be satisfied at the interface $z = 0$.

$$
\begin{cases}
\rho_1 G_2 = \rho_2 G_3 \\
dG_2 / dz = dG_3 / dz
\end{cases} \quad at\ z = 0 \tag{10}
$$

In addition, we impose the continuity of pressure and discontinuity of vertical particle velocity on the plane $z = d$ at the depth of the source.

$$
\begin{cases}
G_1 = G_2 \\
\dfrac{dG_2}{dz} - \dfrac{dG_1}{dz} = 2
\end{cases} \quad at\ z = d \tag{11}
$$

The particle velocity of the point source is assumed to be 2 instead of 1 to simplify the calculation.

These conditions can be represented in a matrix form, and we obtain

$$\begin{pmatrix} 0 & \rho_1 & \rho_1 & -\rho_2 \\ 0 & -\beta_1 & \beta_1 & -\beta_2 \\ e^{-i\beta_1 d} & -e^{-i\beta_1 d} & -e^{i\beta_1 d} & 0 \\ e^{-i\beta_1 d} & -e^{-i\beta_1 d} & e^{i\beta_1 d} & 0 \end{pmatrix} \begin{pmatrix} A \\ B \\ C \\ D \end{pmatrix} = \begin{pmatrix} 0 \\ 0 \\ 0 \\ 2/i\beta_1 \end{pmatrix} \tag{12}$$

Each coefficient is determined by solving the matrix. Using Cramer's rule, we obtain

$$\begin{aligned} A &= \frac{1}{i\beta_1}\left( e^{i\beta_1 d} + \left( \frac{\beta_1 - b\beta_2}{\beta_1 + b\beta_2} \right) e^{-i\beta_1 d} \right) \\ B &= \frac{1}{i\beta_1}\left( \frac{\beta_1 - b\beta_2}{\beta_1 + b\beta_2} \right) e^{-i\beta_1 d} \\ C &= \frac{1}{i\beta_1} e^{-i\beta_1 d} \\ D &= \frac{1}{i\beta_1}\left( \frac{2b\beta_1}{\beta_1 + b\beta_2} \right) e^{-i\beta_1 d} \end{aligned} \tag{13}$$

where $b = \rho_1 / \rho_2$ , density ratio.

With each coefficient, $G(z)$ can be determined as

$$\begin{aligned} G_1(z) &= \frac{1}{i\beta_1}\left( e^{i\beta_1 d} + \left( \frac{\beta_1 - b\beta_2}{\beta_1 + b\beta_2} \right) e^{-i\beta_1 d} \right) e^{-i\beta_1 z} \\ G_2(z) &= \frac{1}{i\beta_1}\left( \frac{\beta_1 - b\beta_2}{\beta_1 + b\beta_2} \right) e^{-i\beta_1 d} e^{-i\beta_1 z} + \frac{1}{i\beta_1} e^{-i\beta_1 d} e^{i\beta_1 z} \\ G_3(z) &= \frac{1}{i\beta_1}\left( \frac{2b\beta_1}{\beta_1 + b\beta_2} \right) e^{-i\beta_1 d} e^{i\beta_2 z} \end{aligned} \tag{14}$$

Consequently, substituting equation (14) into equation (8) and integrating from $-\infty$ to $\infty$ with respect to $k$, we obtain the velocity potential in each region.

$$
\begin{aligned}
u_1 = e^{i\omega t}\phi_1(x,z,\omega) &= e^{i\omega t}\int_{-\infty}^{\infty}\frac{1}{i\beta_1}e^{\pm ikx}e^{-i\beta_1(z-d)}dk \\
&\quad + e^{i\omega t}\int_{-\infty}^{\infty}\frac{1}{i\beta_1}\left(\frac{\beta_1-b\beta_2}{\beta_1+b\beta_2}\right)e^{\pm ikx}e^{-i\beta_1(z+d)}dk \\
u_2 = e^{i\omega t}\phi_2(x,z,\omega) &= e^{i\omega t}\int_{-\infty}^{\infty}\frac{1}{i\beta_1}e^{\pm ikx}e^{-i\beta_1(d-z)}dk \\
&\quad + e^{i\omega t}\int_{-\infty}^{\infty}\frac{1}{i\beta_1}\left(\frac{\beta_1-b\beta_2}{\beta_1+b\beta_2}\right)e^{\pm ikx}e^{-i\beta_1(d+z)}dk \\
u_3 = e^{i\omega t}\phi_3(x,z,\omega) &= e^{i\omega t}\int_{-\infty}^{\infty}\frac{1}{i\beta_1}\left(\frac{2b\beta_1}{\beta_1+b\beta_2}\right)e^{\pm ikx}e^{-i(\beta_1 d-\beta_2 z)}dk
\end{aligned}
\tag{15}
$$

The first integral of $u_1$ and $u_2$ implies a direct wave from the source to the receiver, and the second denotes the refraction and reflection wave events. The integral of $u_3$ involves a wave traveling across the interface between two media. The second integral of $u_1$ and $u_2$ are identical, but the first integrals of $u_1$ and $u_2$ are different in terms of the signs of $z$ and $d$, depending on the position of the source and the receiver. The quantity in parentheses of $u_1$ and $u_2$ is the Rayleigh reflection coefficient, which indicates the energy ratio rebounded from the boundary to the lower medium. The quantity in parentheses of $u_3$ is the Rayleigh refraction coefficient, which indicates the energy ratio transmitted to the upper medium. In this paper, we only consider the case involving a refraction wave (head wave).

To visualize the wave motion, we generated the seismogram for the velocity potential $u_2$ using computer arithmetic. Because $u_2$ is given in the frequency-wavenumber domain, we obtained a solution in time-space by taking two-dimensional inverse Fourier transforms in terms of $k$ and $\omega$. The Figure 2 shows a seismogram on the two-dimensional plane.

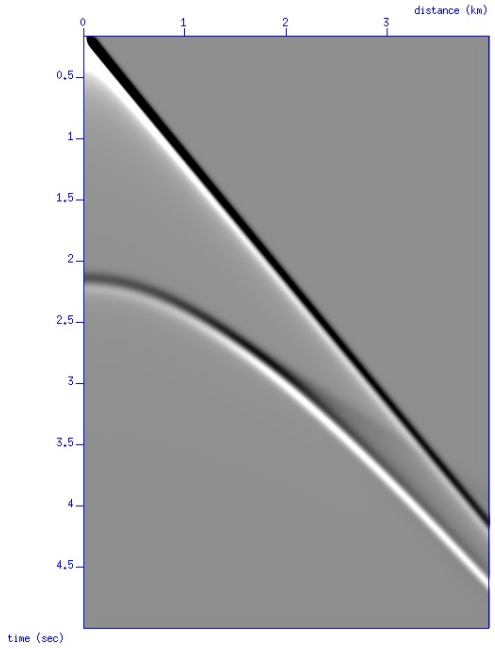


Figure 2. A seismogram of $u_2$. Using the algorithm of inverse Fourier transforms, the solution in the time-space domain can be obtained.

The depth of the source and array of receivers is 1 km from the interface, and the offset varies from 0 km to 4 km along the x-axis. The first derivative of the Gaussian function was applied as a source wavelet. The velocities of the top and bottom layers are 2 and 1 km/s, respectively. We clearly observe a direct wave, a reflection wave, and a refraction wave (head wave).

The Figure 3 shows the snapshots on the two-dimensional plane.

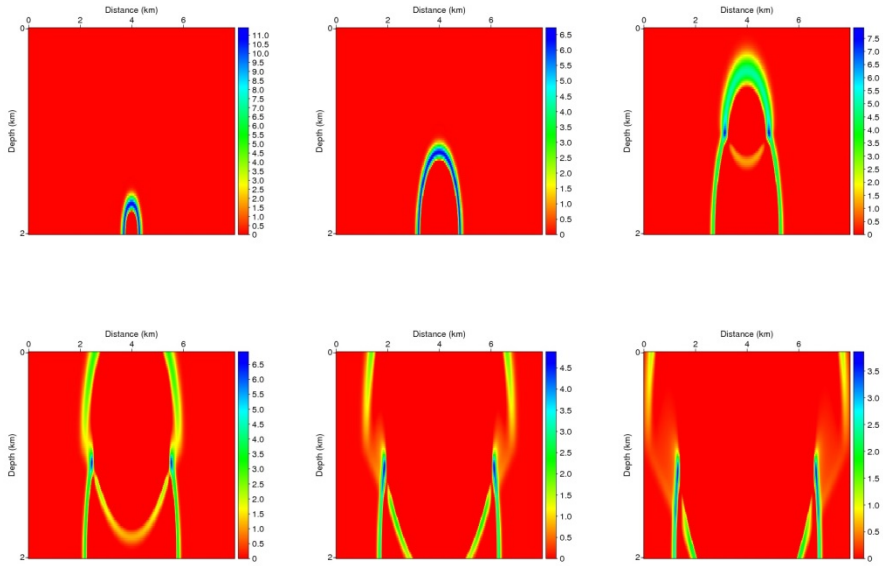


Figure 3. Snapshots of wave motions in the two-dimensional plane.

The source is positioned at a depth of 1.0 km from the boundary. 8.0 km x 2.0 km domain with of interval of 20 m is considered for observing the wave motions. The source wavelet was the first derivative of the Gaussian function. The signal was recorded for 5.0 seconds at an interval of 0.001 second. Each section is at 0.5 second, 1.0 second, 1.5 second, 2.0 second, 2.5 second, and 3.0 second.

Only direct wave is observed for the first time. The reflection wave occurs after the wave reflects from the interface. In particular, a head wave appears in the distance far from the critical distance. To further inspect the critical angle and critical distance, the reflection and transmission energy ratio is plotted in Figure 4.


Figure 4. Energy ratio of the reflection and refraction waves relative to the total energy.

The green and red lines are the energy ratios of the refraction and reflection wave, respectively. When the incident angle is larger than the critical angle of $\pi/6$, the reflection wave contains all the energy from the source. Therefore, if the incident angle is larger than the critical angle, only reflection occurs.

Given the geometry, the critical angle and critical distance can be obtained from Snell's law. Thus, the critical angle is $\pi/6$, and the critical distance is 1.15 km, which corresponds to the computed results shown in Figure 5.

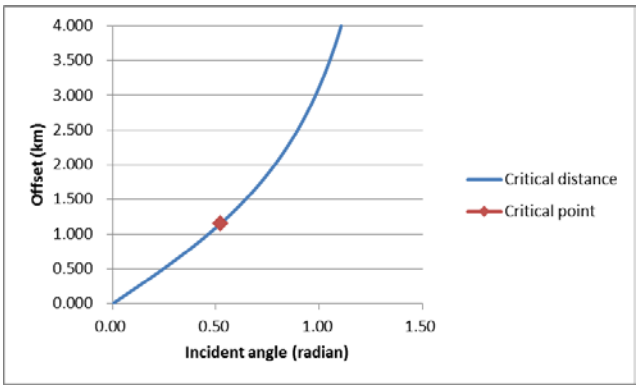


Figure 5. Critical distance at the critical angle under the given circumstances.

To verify the accuracy of the analytic solution, we compared it with the numerical modeling result. Given an identical geometry, numerical finite element modeling was performed in the time-space domain. Figure 6 compares three traces at the receiver positioned 1.0, 2.0, and 3.0 km from the source. There is a big difference between trace from analytic solution and numerical modeling. Thus, each trace is normalized by each maximum value.

(a)

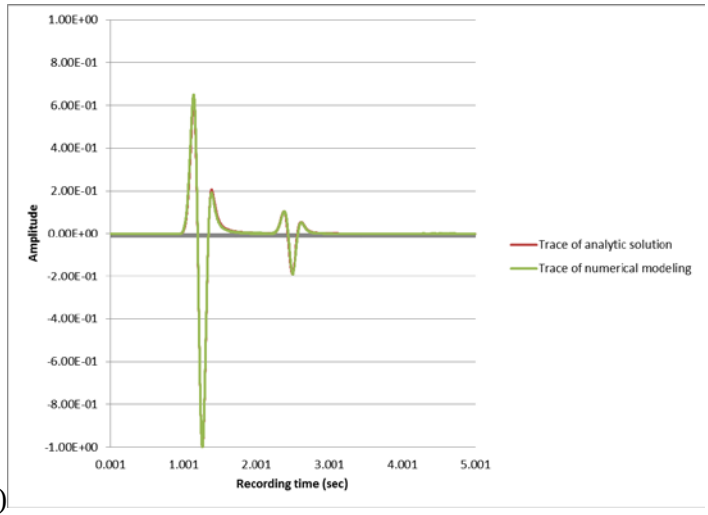


(b)

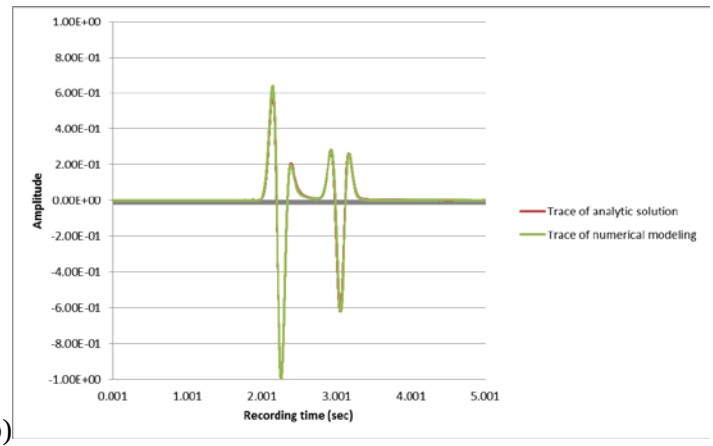


(c)

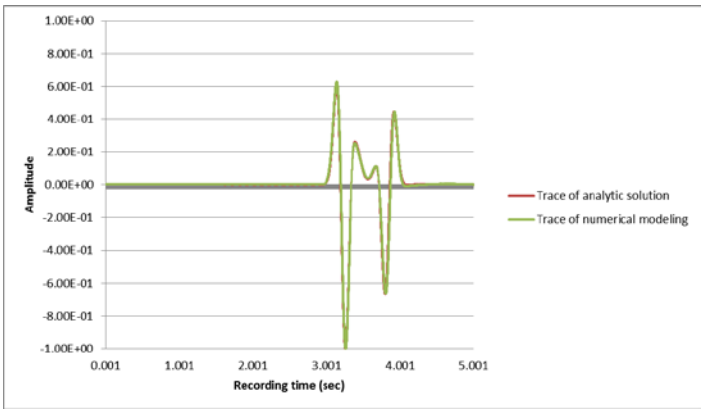


Figure 6. Two traces at the receiver located 1.0 km (a), 2.0 km (b), and 3.0 km (c) from the source. Only negligible error exists between the two traces.

The characteristic of wave events in plane domain is different from that in three-dimensional domain. Thus, we derived each wave event mathematically.

The first integral of $u_1$ and $u_2$, which represents the direct wave, can be easily expressed as

$$\int_{-\infty}^{\infty} \frac{1}{i\beta_1} e^{\pm ikx} e^{-i\beta_1(d-z)} dk = \frac{1}{\sqrt{x^2+(z-d)^2}} e^{-ik_1\sqrt{x^2+(z-d)^2}} \qquad (16)$$

The integral has a direct straight path from the source to a receiver and the decay in wave amplitude is inversely proportional to the square root of the distance. The analytic solution for the reflection wave near the source can be found in many other papers. Hence, we confine the problem to where the offset is larger than the critical distance and the incident angle is larger than the critical angle. The reflection and refraction waves can be derived by performing the complex integral of the second integral of $u_1$ and $u_2$ for a high-speed upper medium.

## 2.3 Evaluation of resultant integral for long ranges

Before performing the contour integration, the second integral term can be written as follows.

Using the property of evenness and oddness of the given function, we obtain

$$u_2 = e^{i\omega t}\phi_2(x,z,\omega) = e^{i\omega t}\int_{-\infty}^{\infty}\frac{1}{i\beta_1}e^{\pm ikx}e^{-i\beta_1(d-z)}dk + e^{i\omega t}\int_{-\infty}^{\infty}\frac{1}{i\beta_1}\left(\frac{\beta_1-b\beta_2}{\beta_1+b\beta_2}\right)e^{\pm ikx}e^{-i\beta_1(d+z)}dk$$

$$\begin{aligned}\varphi_2 &= \int_{-\infty}^{\infty}\frac{1}{i\beta_1}\left(\frac{\beta_1-b\beta_2}{\beta_1+b\beta_2}\right)e^{\pm ikx}e^{-i\beta_1(d+z)}dk \\ &= \int_{-\infty}^{\infty}\{\cos(kx)\pm i\sin(kx)\}\frac{1}{i\beta_1}\left(\frac{\beta_1-b\beta_2}{\beta_1+b\beta_2}\right)e^{-i\beta_1(d+z)}dk \\ &= 2\int_0^{\infty}\cos(kx)\frac{1}{i\beta_1}\left(\frac{\beta_1-b\beta_2}{\beta_1+b\beta_2}\right)e^{-i\beta_1(d+z)}dk \\ &(\because \textit{evenness and oddness in terms of } k) \\ &= 2\int_0^{\infty}\frac{e^{ikx}+e^{-ikx}}{2}\frac{1}{i\beta_1}\left(\frac{\beta_1-b\beta_2}{\beta_1+b\beta_2}\right)e^{-i\beta_1(d+z)}dk \\ &(\because \cos kx = \frac{e^{ikx}+e^{-ikx}}{2}) \\ &= \int_0^{\infty}\left(e^{ikx}+e^{-ikx}\right)\frac{1}{i\beta_1}\left(\frac{\beta_1-b\beta_2}{\beta_1+b\beta_2}\right)e^{-i\beta_1(d+z)}dk\end{aligned} \tag{17}$$

Now, let us perform the contour integration to theoretically evaluate these seismic events. There are no poles, but two branch points in the given integral (See Appendix A). Thus, like Pekeris, Officer, and Ewing, we take the branch lines as shown in Figure 7 (Pekeris, 1948; Officer, 1958; Ewing et al, 1957)

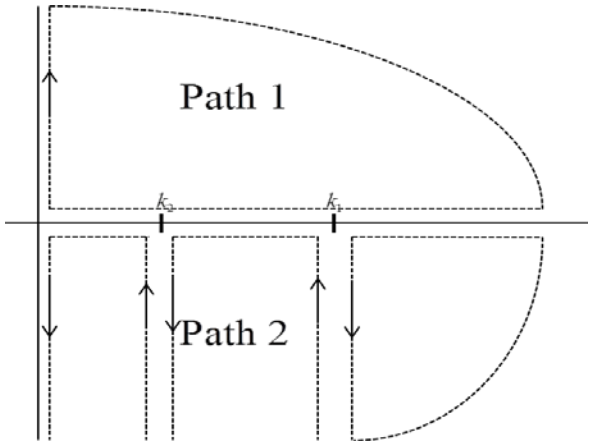


Figure 7. : Path of contour integration for the second integral of $u_1$ and $u_2$

The path of contour integration is identical to that of Pekeris. To avoid the branch points, the path is set as above. Path 1 remains only in the first quadrant and Path 2 remains only in the fourth quadrant. Thus, neither of paths crosses the branch points. $e^{ikx}$ is taken as an infinite term in the first quadrant and $e^{-ikx}$ is taken as an infinite term in the fourth quadrant to satisfy the problem condition.

Path 1:

$$\int_0^{\infty} e^{ikx}\frac{1}{i\beta_1}\left(\frac{\beta_1-b\beta_2}{\beta_1+b\beta_2}\right)e^{-i\beta_1(d+z)}dk=\int_0^{i\infty} e^{ikx}\frac{1}{i\beta_1}\left(\frac{\beta_1-b\beta_2}{\beta_1+b\beta_2}\right)e^{-i\beta_1(d+z)}dk+\lim_{k\to\infty}\int_{i\infty}^{0} e^{ikx}\frac{1}{i\beta_1}\left(\frac{\beta_1-b\beta_2}{\beta_1+b\beta_2}\right)e^{-i\beta_1(d+z)}dk \tag{18}$$

Path 2:

$$\begin{aligned}\int_0^{\infty} e^{-ikx}\frac{1}{i\beta_1}\left(\frac{\beta_1-b\beta_2}{\beta_1+b\beta_2}\right)e^{-i\beta_1(d+z)}dk=&\int_0^{-i\infty} e^{-ikx}\frac{1}{i\beta_1}\left(\frac{\beta_1-b\beta_2}{\beta_1+b\beta_2}\right)e^{-i\beta_1(d+z)}dk\\&+\lim_{k\to\infty}\int_{-i\infty}^{0} e^{ikx}\frac{1}{i\beta_1}\left(\frac{\beta_1-b\beta_2}{\beta_1+b\beta_2}\right)e^{-i\beta_1(d+z)}dk\\&+\int_{k_1}^{-i\infty} e^{-ikx}\frac{1}{i\beta_1}\left(\frac{\beta_1-b\beta_2}{\beta_1+b\beta_2}\right)e^{-i\beta_1(d+z)}dk\\&+\int_{-i\infty}^{k_1} e^{-ikx}\frac{1}{i\beta_1}\left(\frac{\beta_1-b\beta_2}{\beta_1+b\beta_2}\right)e^{-i\beta_1(d+z)}dk\\&+\int_{k_2}^{-i\infty} e^{-ikx}\frac{1}{i\beta_1}\left(\frac{\beta_1-b\beta_2}{\beta_1+b\beta_2}\right)e^{-i\beta_1(d+z)}dk\\&+\int_{-i\infty}^{k_2} e^{-ikx}\frac{1}{i\beta_1}\left(\frac{\beta_1-b\beta_2}{\beta_1+b\beta_2}\right)e^{-i\beta_1(d+z)}dk\end{aligned} \tag{19}$$

The original term is the sum of the integrals of path 1 and 2. The first integrals of path 1 and 2 cancel each other out. The second integrals of path 1 and 2 vanish at $\infty$ in the first and fourth quadrants, respectively. Consequently, the reflection wave and head wave can be derived from the

four left integrals. Two integrands in terms of $k_1$ of the four left integrals imply the reflection wave, and the other two in terms of $k_2$ represent the head wave. Thus, we have

$$\int_{k_1}^{-i\infty} e^{-ikx}\frac{1}{i\beta_1}\left(\frac{\beta_1-b\beta_2}{\beta_1+b\beta_2}\right)e^{-i\beta_1(d+z)}dk+\int_{-i\infty}^{k_1} e^{-ikx}\frac{1}{i\beta_1}\left(\frac{\beta_1-b\beta_2}{\beta_1+b\beta_2}\right)e^{-i\beta_1(d+z)}dk$$
$$+\int_{k_2}^{-i\infty} e^{-ikx}\frac{1}{i\beta_1}\left(\frac{\beta_1-b\beta_2}{\beta_1+b\beta_2}\right)e^{-i\beta_1(d+z)}dk+\int_{-i\infty}^{k_2} e^{-ikx}\frac{1}{i\beta_1}\left(\frac{\beta_1-b\beta_2}{\beta_1+b\beta_2}\right)e^{-i\beta_1(d+z)}dk$$
$$=\int_{k_1,-i\infty}^{k_1} e^{-ikx}\left[F(\beta_1,\beta_2)-F(-\beta_1,\beta_2)\right]dk+\int_{k_2,-i\infty}^{k_2} e^{-ikx}\left[F(\beta_1,\beta_2)-F(\beta_1,-\beta_2)\right]dk \tag{20}$$

$$where\quad F(\beta_1,\beta_2)=\frac{1}{i\beta_1}\left(\frac{\beta_1-b\beta_2}{\beta_1+b\beta_2}\right)e^{-i\beta_1(z+d)}$$

The integrands involving exponential function diverge to zero when the imaginary part of $k$ is large negative. Thus, only the value near real axis is considered for contour integration.

### 2.3.1 Evaluation of reflection wave

First, let us evaluate the reflection wave. The integrand in terms of $k_1$ is

$$\varphi_{k_1} = \int_{k_1,-i\infty}^{k_1} e^{-ikx}\left[F(\beta_1,\beta_2) - F(-\beta_1,\beta_2)\right]dk \tag{21}$$

Because $x$ is sufficiently larger than the critical distance, let us consider the small imaginary part of $k$ near a branch point $k_1$.

$$k = k_1\lambda \qquad where\ \lambda = 1 - iu \tag{22}$$

Then, for a small value of $u$, we have

$$k = k_1\lambda \approx k_1$$
$$dk = -ik_1 du$$
$$\beta_1 = \sqrt{k_1^2 - k^2} = \sqrt{k_1^2 - k_1^2\lambda^2} = k_1\sqrt{1-\lambda^2} \approx k_1\sqrt{2iu} = k_1\sqrt{2u}e^{i(\pi/4)}$$
$$\beta_2 = \sqrt{k_2^2 - k^2} = k_1\sqrt{\frac{c_1^2}{c_2^2} - \lambda^2} \approx k_1\sqrt{\frac{c_1^2}{c_2^2} - 1} \approx ik_1\sqrt{1 - \frac{c_1^2}{c_2^2}} = ik_1\mu$$
$$where \quad \mu = \sqrt{1 - \frac{c_1^2}{c_2^2}}$$
$$F(\beta_1,\beta_2) - F(-\beta_1,\beta_2) = \frac{1}{i\beta_1}\left(\frac{\beta_1 - b\beta_2}{\beta_1 + b\beta_2}\right)e^{-i\beta_1(z+d)} - \frac{1}{-i\beta_1}\left(\frac{-\beta_1 - b\beta_2}{-\beta_1 + b\beta_2}\right)e^{i\beta_1(z+d)}$$
$$= \frac{2}{i\beta_1}\left\{\frac{\left(\beta_1^2 + b^2\beta_2^2\right)\cos\left[\beta_1\left(z+d\right)\right] + 2ib\beta_1\beta_2\sin\left[\beta_1\left(z+d\right)\right]}{\beta_1^2 - b^2\beta_2^2}\right\}$$
$$\approx \frac{-2e^{-i(\pi/4)}}{ik_1\sqrt{2u}}\left\{\cos(m\sqrt{u}) + \frac{2\sqrt{2x}e^{i(\pi/4)}}{b\mu}\sin\left(m\sqrt{u}\right)\right\}$$
$$where \quad m = \sqrt{2}k_1e^{i(\pi/4)}(z+d) \tag{23}$$

Substituting the variable which is parameterized with $k_1$ into $\varphi_{k_1}$, $\varphi_{k_1}$ becomes

$$\begin{aligned}\varphi_{k_1} &= \int_{\infty}^{0} e^{-ikx}\frac{-2e^{-i(\pi/4)}}{ik_1\sqrt{2u}}\left[\cos(m\sqrt{u})+\frac{2\sqrt{2u}e^{i(\pi/4)}}{b\mu}\sin(m\sqrt{u})\right](-ik_1du)\\ &= \int_{\infty}^{0} e^{-ikx}\frac{-2e^{-i(\pi/4)}}{ik_1\sqrt{2u}}\cos(m\sqrt{u})(-ik_1du)\\ &\qquad + \int_{\infty}^{0} e^{-ikx}\frac{-2e^{-i(\pi/4)}}{ik_1\sqrt{2u}}\frac{2\sqrt{2u}e^{i(\pi/4)}}{b\mu}\sin(m\sqrt{u})(-ik_1du)\\ &= \int_{0}^{\infty} e^{-ikx}\frac{-2e^{-i(\pi/4)}}{\sqrt{2u}}\cos(m\sqrt{u})(du)-\int_{0}^{\infty} e^{-ikx}\frac{4}{b\mu}\sin(m\sqrt{u})(du)\end{aligned} \tag{24}$$

Because $e^{-ikx}=e^{-ik_1(1-iu)x}=e^{-ik_1x}e^{-k_1xu}$, equation (24) can be written as

$$\varphi_{k_1}=\int_{0}^{\infty} e^{-ik_1x}e^{-k_1xu}\frac{-2e^{-i(\pi/4)}}{\sqrt{2u}}\cos(m\sqrt{u})(du)-\int_{0}^{\infty} e^{-ik_1x}e^{-k_1xu}\frac{4}{b\mu}\sin(m\sqrt{u})(du)$$

Let us change a variable of integration to $v$, where $u=v^2$. Then, we have

$$\begin{aligned}\varphi_{k_1} &= -2\sqrt{2}e^{-i(\pi/4)}e^{-ik_1x}\int_{0}^{\infty} e^{-k_1xv^2}\cos(mv)dv-\frac{8}{b\mu}e^{-ik_1x}\int_{0}^{\infty} e^{-k_1xv^2}\sin(mv)dv\\ &= -2\sqrt{2}e^{-i(\pi/4)}e^{-ik_1x}\frac{\sqrt{\pi}e^{-\frac{m^2}{4k_1x}}}{2\sqrt{k_1x}}-\frac{8}{b\mu}e^{-ik_1x}\frac{m}{2k_1x}\frac{\sqrt{\pi}e^{-\frac{m^2}{4k_1x}}}{2\sqrt{k_1x}}\\ &= -\frac{\sqrt{2\pi}e^{-i(\pi/4)}}{\sqrt{k_1x}}e^{-ik_1x}e^{-\frac{m^2}{4k_1x}}-\frac{2m\sqrt{\pi}}{b\mu k_1x\sqrt{k_1x}}e^{-ik_1x}e^{-\frac{m^2}{4k_1x}}\end{aligned} \tag{25}$$

Now, we have

$$\varphi_{k_1} = e^{-ik_1 x} e^{-\frac{m^2}{4k_1 x}} \frac{\sqrt{\pi}}{\sqrt{k_1 x}} \left[ \sqrt{2} e^{-i(\pi/4)} + \frac{2m}{b\mu k_1 x} \right] \tag{26}$$

Assuming that $x$ is sufficiently large, the term with $1/x$ is negligible.

Thus, the approximated solution is

$$\varphi_{k_1} = e^{-ik_1 x} e^{-\frac{m^2}{4k_1 x}} \frac{\sqrt{2\pi} e^{-i(\pi/4)}}{\sqrt{k_1 x}} = \frac{\sqrt{2\pi i}}{\sqrt{k_1 x}} e^{-ik_1 \left( x + \frac{(z+d)^2}{2x} \right)} \tag{27}$$

With the first two terms of the series expansion, the exponential term is expressed as

$$\sqrt{x^2 + (z+d)^2} = x \left[ 1 + \frac{(z+d)^2}{x^2} \right]^{1/2} = x \left[ 1 + \frac{(z+d)^2}{2x^2} \right]^{1/2} \tag{28}$$

Consequently,

$$\varphi_{k_1} = \frac{\sqrt{2\pi i}}{\sqrt{k_1 x}} e^{-ik_1 (x^2 + (z+d)^2)^{1/2}} \tag{29}$$

The exponential term shows the reflection ray path from Snell's law. A phase change of $\pi$ occurs in the equation. The amplitude of the reflection wave in the two-dimensional plane domain is proportional to the inverse of the square root of the distance between the source and the receiver. To verify this fact, we performed a regression analysis. Although we should pick up certain amplitude points on the reflection event, the wave amplitude varied for a few milliseconds at each receiver. Thus, we selected the strongest signal at each receiver. Then, random receiver points were selected and we attempted to fit them to a polynomial of $1/\sqrt{x}$. Figure 8 shows the result.

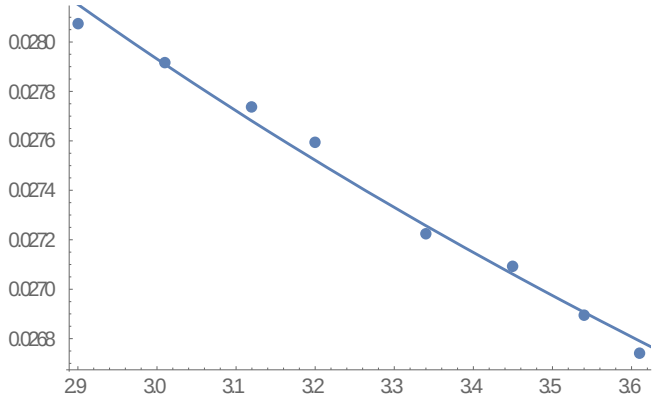


Figure 8. : Polynomial fitting of the amplitude point of the reflection wave to the function of $1/\sqrt{x}$ .

The amplitude points on the reflection events are well-fitted to the given polynomial function. The receivers were randomly selected to check the amplitude pattern to distance $x$. Then, 8 random points were selected as a sample and we used the regression analysis module of Mathematica to perform the regression analysis. These results are well-fitted to the function of $1/\sqrt{x}$ , and the coefficient of determination is 0.985.

Furthermore, the amplitude of the reflection wave is related to the angular frequency $\omega$. Although the amplitude of the analytic solution in three dimensions is independent of $\omega$ (Pekeris, 1948), the amplitude in two dimensions is proportional to the inverse of the square root of $\omega$. To verify this trend, we recorded the angular frequency spectrum of the reflection wave at a receiver, and attempted to fit it to a polynomial of $1/\sqrt{\omega}$. Figure 9 shows the relationship between the amplitude and $\omega$.

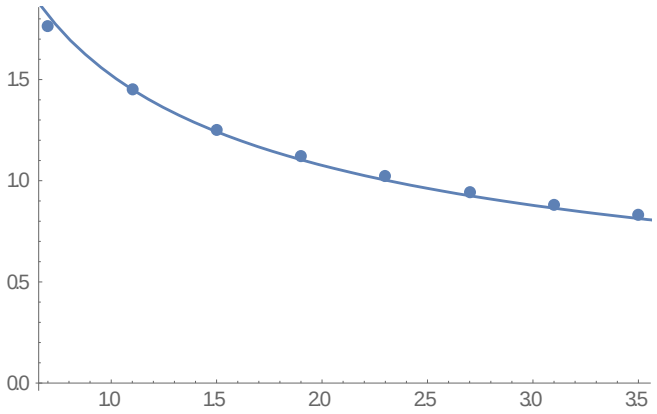


Figure 9. : Polynomial fitting of the angular frequency spectrum to the function of $1/\sqrt{\omega}$.

The receiver 1.5 km from the source was selected for a regression analysis. The spectrum was recorded from 0.7 Hz to 3.5 Hz at an interval of 0.4 Hz. The results are well-fitted to the function of $1/\sqrt{\omega}$, and the coefficient of determination is 0.998.

### 2.3.2 Evaluation of refraction wave

By performing the contour integration in terms of $k_2$, the head wave can be invented. The integrand in terms of $k_2$ is

$$\varphi_{k_2} = \int_{k_2,-i\infty}^{k_2} e^{-ikx}\left[F(\beta_1,\beta_2) - F(\beta_1,-\beta_2)\right]dk \tag{30}$$

Using the previous procedure for $\varphi_{k_1}$, let us assume

$$k = k_1\eta \qquad where\ \ \eta = \frac{c_1}{c_2} - iu \tag{31}$$

Then, for a small value of $u$, we have

$$k = k_1\eta \approx k_1\frac{c_1}{c_2} = k_2$$

$$dk = -ik_1 du$$

$$\beta_1 = \sqrt{k_1^2 - k^2} = k_1\sqrt{1-\eta^2} \approx k_1\left(1-\frac{c_1^2}{c_2^2}\right)^{1/2} = k_1\mu$$

$$\beta_2 = \sqrt{k_2^2 - k^2} = k_1\left(\frac{c_1^2}{c_2^2} - \eta^2\right)^{1/2} \approx k_1\left(2iu\frac{c_1}{c_2}\right)^{1/2}$$

$$F(\beta_1,\beta_2) - F(\beta_1,-\beta_2) = \frac{1}{i\beta_1}\left(\frac{\beta_1 - b\beta_2}{\beta_1 + b\beta_2}\right)e^{-i\beta_1(z+d)} - \frac{1}{i\beta_1}\left(\frac{\beta_1 + b\beta_2}{\beta_1 - b\beta_2}\right)e^{-i\beta_1(z+d)}$$

$$= \frac{4ib\beta_2}{\beta_1^2 - b^2\beta_2^2}e^{-i\beta_1(z+d)}$$

$$\approx \frac{4ib\sqrt{2iu(c_1/c_2)}}{k_1\mu^2}e^{-ik_1\mu(z+d)} \tag{32}$$

Substituting the variable that was parameterized with $k_2$ into $\varphi_{k_2}$, $\varphi_{k_2}$ becomes

$$\begin{aligned}\varphi_{k_2} &= \int_{\infty}^{0} e^{-ikx}\frac{4ib(2uc_1/c_2)^{1/2}e^{i(\pi/4)}}{k_1\mu^2}e^{-ik_1\mu(z+d)}(-ik_1du)\\ &= -\frac{4\sqrt{2}b(c_1/c_2)^{1/2}e^{i(\pi/4)}}{k_1\mu^2}e^{-ik_1\mu(z+d)}\int_0^{\infty}e^{-iku}\sqrt{u}du\end{aligned} \tag{33}$$

Because $e^{-ikx} = e^{-ik_1(\frac{c_1}{c_2}-iu)x} = e^{-ik_2x}e^{-k_1xu}$, equation (33) can be rewritten as

$$\begin{aligned}\varphi_{k_2} &= -\frac{4\sqrt{2}b(c_1/c_2)^{1/2}}{\mu^2}e^{-ik_1\mu(z+d)}e^{-ik_2x}\int_0^{\infty}e^{-k_1xu}\sqrt{u}du\\ &= -\frac{4\sqrt{2}b(c_1/c_2)^{1/2}}{\mu^2}e^{-ik_1\mu(z+d)}e^{-ik_2x}\left[\frac{\sqrt{\pi}}{2(k_1x)^{3/2}}\right]\\ &= -\frac{2\sqrt{2}b(c_1/c_2)^{1/2}}{\mu^2}\frac{\sqrt{\pi}}{(k_1x)^{3/2}}e^{-i(k_2x+k_1\mu(z+d))}\end{aligned} \tag{34}$$

Consequently,

$$\begin{aligned}\varphi_{k_2} &= -\frac{2\sqrt{2\pi}b\sqrt{k_1c_1/c_2}}{\mu^2(k_1x)^{3/2}}e^{-i(k_2x+k_1\mu(z+d))}\\ &= -\frac{2\sqrt{2\pi}b\sqrt{k_2}}{\mu^2k_1^2x^{3/2}}e^{-i(k_2x+k_1\mu(z+d))}\end{aligned} \tag{35}$$

Unlike the direct and reflection waves, the head wave includes a $k_2$ term. The exponential term, which implies the travel time of wave, has both $k_1$ and $k_2$. Thus, some part of the path propagates with velocity $c_1$, and the other part propagates with velocity $c_2$. From the work of Pekeris, who rewrote the exponent term with the critical angle (Pekeris, 1948), we can know that the wave enters at the critical angle and reflects out at the critical

angle.

$$
\begin{aligned}
k_2 r + k_1 \mu (z+d) &= \omega \left[ \frac{x}{c_2} + \frac{z+d}{c_1} \left( 1 - \frac{c_1^2}{c_2^2} \right)^{1/2} \right] \\
&= \omega \left[ \frac{x}{c_2} + \frac{z+d}{c_1} \cos\theta_c \right] \\
&= \omega \left[ \frac{x-(z+d)\tan\theta_c}{c_2} + \frac{z+d}{c_1} \left( \cos\theta_c + \frac{c_1}{c_2} \tan\theta_c \right) \right] \\
&= \omega \left[ \frac{x-(z+d)\tan\theta_c}{c_2} + \frac{z+d}{c_1} \left( \frac{\cos^2\theta_c + \sin^2\theta_c}{\cos\theta_c} \right) \right] \\
&= \omega \left[ \frac{x-(z+d)\tan\theta_c}{c_2} + \frac{(z+d)/\cos\theta_c}{c_1} \right]
\end{aligned}
\tag{36}
$$

Additionally, the amplitude of the head wave in the two-dimensional plane domain is proportional to the inverse of $x^{3/2}$, where the distance is $x$. As previously implemented, the amplitude points were selected as a sample for a regression analysis. Figure 10 shows the results of fitting to the polynomial of $1/x^{3/2}$.

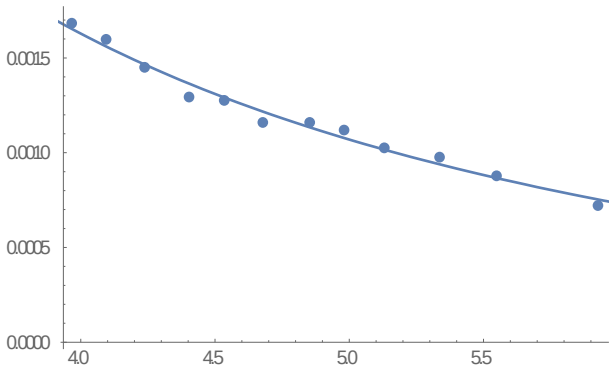


Figure 10. : Polynomial fitting of the amplitude point of the head wave to the function of $1/x^{3/2}$.

The strongest signal of the refraction event was selected to implement a regression analysis. The receivers were randomly selected to check the amplitude pattern to distance $x$. Then, 12 random points were selected as a sample and we used a regression analysis module in the Mathematica program to perform the analysis. The results are well-fitted to the function of $1/x^{3/2}$, and the coefficient of determination is 0.982.

In addition, the amplitude of the head wave is related to the angular frequency $\omega$. Although the amplitude of the analytic solution in three dimensions is proportional to the inverse of $\omega$ (Pekeris, 1948), the amplitude in two dimensions is proportional to the inverse of $\omega^{3/2}$. To verify this trend, we recorded the angular frequency spectrum of the head wave at a receiver, and attempted to fit it to a polynomial of $1/\omega^{3/2}$. Figure 11 shows the relationship between the amplitude and $\omega$.

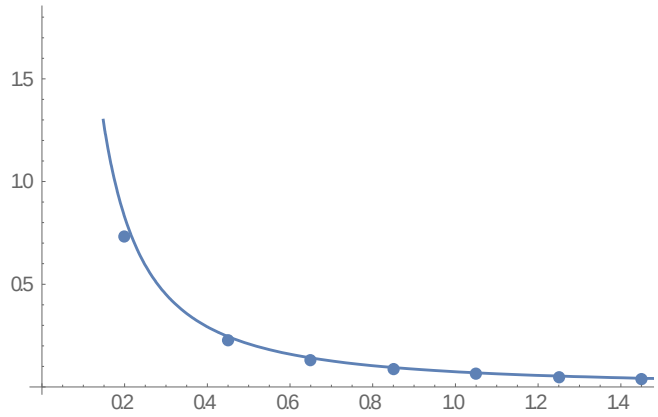


Figure 11. : Polynomial fitting of the amplitude point of the head wave to the function of $1/\omega^{3/2}$.

The receiver 1.5 km from the source was selected for a regression analysis. The spectrum was recorded from 0.05 Hz to 1.5 Hz at an interval of 0.25 Hz. These results are well-fitted to the function of $1/\omega^{3/2}$ and the coefficient of determination is 0.923.

We also attached table 1 to compare the two-dimensional and three-dimensional solutions.

| | 2D solution | 3D solution |
|---|---|---|
| **Reflection wave** | | |
| Term of integrand | Exponential function | Hankel function |
| Relation between amplitude and distance $(x)$ | $Amp \propto 1/\sqrt{x}$ | $Amp \propto 1/x$ |
| Relation between amplitude and angular frequency $(\omega)$ | $Amp \propto 1/\sqrt{\omega}$ | Independent |
| **Head wave** | | |
| Term of integrand | Exponential function | Hankel function |
| Relation between amplitude and distance $(x)$ | $Amp \propto 1/x\sqrt{x}$ | $Amp \propto 1/x^2$ |
| Relation between amplitude and angular frequency $(\omega)$ | $Amp \propto 1/\omega\sqrt{\omega}$ | $Amp \propto 1/\omega$ |

Table 1. Comparison between the two-dimensional and three-dimensional solutions.

# Chapter 3 Conclusion

In this paper, we theoretically solve the problem of acoustic wave propagation in two-dimensional unbounded plane media. Unlike the three-dimensional solution with the Hankel function, which results in difficult numerical integration, the two-dimensional solution with an exponential function can be inverted with the two-dimensional inverse Fourier transform to obtain wave motion in the time-space domain. Furthermore, we visualized the wave propagation in a given geometry using computational arithmetic to allow more intuitive understanding of wave behavior. After a simple operation, we found that the amplitude of the reflection wave in the two-dimensional plane is proportional to the inverse of the square root of the distance and angular frequency, and that of the head wave is proportional to the inverse of the square root of the cube of the distance and angular frequency. With the knowledge from this study, calculation of acoustic wave propagation in a two-dimensional bounded plane medium is feasible.

# Chapter 4 References

Brekhovskikh L. M., and Lysanov Y. P., 1991, Fundamentals of ocean acoustics, 1st edition: Springer.

Buckingham M. J., 1992, Ocean-acoustic propagation models: J. Acoustique.

DeSanto J. A., 1992, Scalar wave theory: Springer.

Dovrin M. B., 1952, Introduction to geophysical prospecting, 1st edition: McGraw-Hill.

Etter P. C., 2013, Underwater acoustic modeling and simulation, 4th edition: CRC press.

Ewing M. B., Jardetzky W. S., and Press F., 1958, Elastic waves in layered media: McGraw Hill.

Jensen F. B., Kuperman W. A., Porter M. B., and Schmidt H., 1997, Computational ocean acoustics, 1st edition: Springer.

Katsnelson B. G. and Prtnikov V. G., 2002, Shallow water acoustics: Springer.

Kennett B., 1983, Seismic wave propagation in stratified media, 1st edition: ANU E press.

Lurton X., 2002, An introduction to underwater acoustics: principles and applications: Springer-Praxis.

Officer C. B., 1958, Introduction to the theory of sound transmission with application in the ocean: McGraw Hill.

Pekeris C. L., 1948, Theory of propagation of explosive source in shallow water: The Geological Society of America Memoir 27.

Pilant W. L., 2012, Elastic waves in the earth: Elsevier.

Pujol J., 2003, Elastic wave propagation and generation in seismology: Cambridge.

Yilmaz O., 2001, Seismic data analysis, 2nd edition: Society of Exploration Geophysicists.

# 초 록

1948년 C.L. Pekeris는 음향 매질 내 파동 전파 이론의 기틀을 마련하였다. 이후로, 음향 매질 내 파동 전파 이론은 지구물리학, 해양학을 비롯한 파동 전파 현상을 다루는 모든 기초 학문의 필수적인 내용으로 자리잡았다. 실제로 그는 원통 좌표계를 도입하여 음향 반무한 매질 내에서의 파의 거동을 수학적으로 풀어냈다. 그가 구한 음향 반무한 매질 내에서의 해는 수학적으로 완벽하나, 베셀 함수와 한켈 함수를 포함하여 이를 컴퓨터 프로그래밍을 통한 수치적 재현에는 많은 어려움이 따른다. 따라서, 3차원 원통 좌표계 대신 2차원 평면 좌표계에 적용하여 이론 해를 다시 도출한다면, 음향 반무한 매질 내에서의 해는 훨씬 간단히 표현 될 수 있다. 따라서, 2차원 평면 내에서의 해를 컴퓨터 프로그래밍을 통해 보다 쉽게 재현 할 수 있고, 이는 파동 전파 이론을 공부하는 학생들에게 큰 도움이 될 것이다. 본 논문에서는 2차원 평면 상에서의 음향 반무한 매질 내 해를 도출하였고, 이를 수치적 모델링 결과와 비교하였으며, 회귀분석을 통해 구한 결과를 검증하였다.

**주요어** : 파동전파이론, 반무한, 음향 매질, 2차원 평면, 복소적분

**학번 : 2014-20528**